Deuteron binding energies and form factors from light-front Hamiltonian field theory

Jason R. Cooke and Gerald A. Miller
Department of Physics, University of Washington, Box 351560, Seattle, Washington 98195-1560
(Received 17 December 2001; published 27 September 2002)

This paper investigates how the breaking of manifest rotational invariance in light-front dynamics affects the binding energy and the form factors of the deuteron. To do this, we derive new light-front nucleon-nucleon one- and two-meson-exchange potentials, and use the potentials to solve for the deuteron wave function and binding energy. We find that including two-meson-exchange (TME) potentials partially repairs the broken rotational invariance of the one-meson-exchange (OME) potential. This is shown by a decrease in the binding energy difference of different m states of the deuteron. We calculate the matrix elements of the electromagnetic current using the deuteron wave functions obtained from the OME and OME+TME potentials. Rotational invariance requires that the matrix elements satisfy an angular condition, but in light-front dynamics that condition is only partially satisfied. The current matrix elements from the OME calculation satisfy the angular condition better than the ones from the OME+TME calculation. The matrix elements of the axial current satisfy the angular condition to the same extent regardless of which wave functions are used for the calculation. Finally, we find that at momentum transfers greater than about 2 GeV^2, the breaking of rotational invariance causes less uncertainty in the computed deuteron form factors than do the uncertainties in the nucleon form factors.

DOI: 10.1103/PhysRevC.66.034002 PACS number(s): 21.45.+v, 03.65.Ge, 03.65.Pm, 11.10.Ef

I. INTRODUCTION

Recent experiments at Thomas Jefferson National Accelerator Facility have measured the $A(Q^2)$ structure function of the deuteron for momentum transfers up to 6 $(\mathrm{GeV}/c)^2$ [1], and measurements for $B(Q^2)$ are planned. Eventually, even higher momentum transfers will be achieved. At such large momentum transfers, a relativistic description of the deuteron is required. Even at lower momentum transfers, a relativistic description is important to understand the details of the form factors. In addition, incorporating relativity is important for the deuteron wave function to transform correctly under boosts to large momentum, which is important for calculating form factors.

One approach that gives a relativistic description of the deuteron is light-front dynamics. This work investigates the consequences of combining light-front dynamics with various nuclear models to calculate bound state wave functions, and uses them to calculate the deuteron form factors.

The utility of the light-front dynamics was first discussed by Dirac [2]. Light-front dynamics makes use of the light-front coordinate system, where a four-vector x^μ is expressed as $x^\mu=(x^+,x^-,x^1,x^2)$, with $x^\pm=x^0\pm x^3$. Although the light-front coordinate system is simply related to the conventional coordinate system by a change of variables, the relation between light-front dynamics and conventional dynamics is very complex. This is because the light-front Hamiltonian [3–5] is obtained by defining the commutation relations and quantization procedure at equal light-front time $(x^+=t_{\mathrm{LF}})$ instead of at equal time $(x^0=t)$. We use the light-front Hamiltonian in a light-front Schrödinger equation to solve for bound states. There are many desirable features of light-front dynamics and the use of light-front coordinates.

First of all, high-energy experiments are naturally described using light-front coordinates. The wave front of a beam of high-energy particles traveling in the (negative) three-direction is defined by a surface where x^+ is (approximately) constant. Such a beam probes the structure of a target described in terms of light-front variables [3,6,7]: the Bjorken x variable used to describe high-energy experiments is simply the ratio of the plus momentum of the struck constituent particle to the total plus momentum (p^+) of the bound state.

Second, the vacuum for a theory with massive particles can be very simple on the light front. This is because all massive particles and antiparticles have positive plus momentum, and the total plus momentum is a conserved quantity. Thus, the naive vacuum (with $p^+=0$) is empty, and diagrams that couple to this vacuum vanish. This greatly reduces the number of nontrivial light-front time-ordered diagrams.

Third, the generators of boosts in the one, two, and plus directions are independent of the interaction, or kinematic. Thus, even when the Hamiltonian is truncated, the wave functions will transform correctly under boosts, a useful feature when calculating form factors at high momentum transfers.

Finally, it is easy to perform relativistic calculations using light-front dynamics. This is partly due to the simplicity of the vacuum, and partly due the the fact that the light-front center-of-momentum variable (defined as $P^+=p_1^+ + p_2^+$) can be cleanly separated from the relative momentum variable for two particles. This allows us to write relativistic equations which have the simple form of a nonrelativistic Schrödinger equation.

One serious drawback of light-front dynamics is that rotational invariance is not manifest in a light front Hamiltonian where the light-front has a fixed orientation [8]. An untruncated light-front Hamiltonian will commute with the total relative angular momentum operator, since the total momentum commutes with the relative momentum. Thus, eigenstates of the full Hamiltonian will also be eigenstates of

the angular momentum. However, as mentioned earlier, a Fock-space truncation of the light-front Hamiltonian typically results in the momentum operator four-vector losing covariance under rotations. (A notable exception to this is the light-front Bakamjian-Thomas construction, which is explained nicely in Ref. [9].) Hence J^2 does not commute with the truncated Hamiltonian, and this implies that the eigenstates of the truncated Hamiltonian will not be eigenstates of the angular momentum. This is particularly important for the deuteron, since its spin is due to the total angular momentum of the state; it does not arise solely from nucleons' spins. The goal of this work is to investigate how this breaking of rotational invariance affects observables, such as the binding energy and form factors of the deuteron.

How will this violation of rotational invariance affect physical observables? One way to observe this violation is to note that on the light front, rotational invariance about the z axis is maintained. This allows us to classify states as eigenstates of J_3 with eigenvalues m. We compare the binding energy of deuteron states (which have $j=1$) with different m values. If the Hamiltonian were rotationally invariant, the energies should be the same; the breaking of rotational invariance causes the energies to be different [10].

Another symptom of the breaking of rotational invariance is that the angular condition (a relation between the matrix elements of the current required by Poincaré symmetry, defined in Sec. III) for the deuteron current is not exactly satisfied [11–15]. This means that different prescriptions for calculating the deuteron form factors from the deuteron current will in principle give different results when light-front dynamics is used. This dependence on the prescription used has caused concern about the validity of applying light-front dynamics to calculate form factors.

One notable feature of this calculation is that it is done entirely with light-front dynamics; no part relies on equal-time dynamics. The covariant Lagrangian generates light-front potentials, which generate light-front wave functions, which are used in a light-front calculation of the deuteron current and form factors. This is different from other approaches which use deuteron wave functions calculated from equal-time dynamics as a starting point [11–18].

This calculation is also distinguished from calculations done with explicitly covariant light-front dynamics (ECLFD), where the orientation of the light-front plane is not fixed, but variable. ECLFD makes rotational invariance explicit by introducing additional degrees of freedom into the equations. This paper examines the degree to which rotational invariance is broken by various truncations of the potentials when the plane orientation is fixed.

Following this introduction, we introduce a model Lagrangian for nuclear physics which includes chiral symmetry [6] in Sec. II. The methods introduced in Refs. [19,20] are generalized for use with this nuclear model. The Hamiltonian is derived and used to calculate new light-front nucleon-nucleon one-meson-exchange (OME) and two-meson-exchange (TME) potentials. The notation and conventions defined in the appendix are used extensively in this section. We have some freedom in how to choose the TME potentials, and we consider several different choices.

In Sec. III we calculate the electromagnetic and axial form factors of the deuteron. Although rotational invariance demands that there be only three independent components of the deuteron current, the light-front calculation of the deuteron current results in four independent components. This is a result of the lack of manifest rotational invariance on the light front. There are several prescriptions for choosing which deuteron current component should be eliminated, and in principle this choice will affect the form factors. We attempt to find currents that transform well enough under rotations so that the choice of ''bad'' component does not matter too much.

We discuss the results of the calculation the deuteron wave functions and binding energies in Sec. IV. We find that by including the TME potentials for the calculation of the deuteron, the binding energy degeneracy is broken by a smaller amount. The results of our search for currents with good transformation properties are also discussed. We find that for most of the currents, the angular condition does not depend strongly on which potential is used to calculate the wave function. The only exception to this is that part of the electromagnetic current which is multiplied by the isoscalar F_1 nucleon form factor satisfies the angular condition much better when using the wave function calculated with the OME potential than with wave function with other potentials. We also find that the major uncertainty in the calculated deuteron form factors at momentum transfers greater than 2 GeV^2 is due not to the prescription used to determine the form factors from the current, but instead is from the uncertainties in the nucleon form factors.

Note that a solution for the deuteron that transforms properly under rotations must have degenerate binding energies and must satisfy the angular condition; however, the converse is not necessarily true. For example, a decrease in the difference of the binding energies indicates, but does not prove, that the rotational properties of the state have improved.

II. REALISTIC NUCLEAR MODEL

We derive a new light-front nucleon-nucleon potential (LFNN) from an effective nuclear Lagrangian. This model is an extension of the light-front model used by Miller and Machleidt [21]. A new feature of this model is that light-front energy dependent denominators are used in the potentials; the denominators used in Ref. [21] are energy independent. The material in this chapter extends on previous work done with the Wick-Cutkosky model [19,20].

A. Model and formalism

Our starting point is an effective nuclear Lagrangian [6] which incorporates a nonlinear chiral model for the pions. The Lagrangian is based on the linear representations of chiral symmetry used by Gursey [22]. It is invariant (in the limit where $m_\pi \to 0$) under chiral transformations. A realistic nuclear Lagrangian must contain some sort of chiral symmetry, since the underlying QCD Lagrangian is chirally symmetric.

The model prescribes the use of nucleons ψ and six mesons: the π, δ [also known as the $a_0(980)$], σ [also known as the $f_0(400-1200)$], η, ρ, and ω mesons. The coupling of each meson to the nucleon is governed by the combination of the meson's spin and isospin. The π and η are pseudoscalars, the ρ and ω are vectors, and the δ and σ are scalars. Under isospin transformations, the π, ρ, and δ are isovector particles while the η, ω, and σ are isoscalar particles.

The use of scalar mesons is meant as a simple representation of part of the two-pion-exchange potential which causes much of the medium range attraction between nucleons [23,24]. It can also be interpreted as the effect of fundamental scalar mesons [25–27].

The Lagrangian $\mathcal{L}$ is based on the one used in Refs. [6,21,28]. It is given by

$$\begin{aligned}\mathcal{L}=&-\frac{1}{4}\boldsymbol{\rho}^{\mu\nu}\cdot\boldsymbol{\rho}_{\mu\nu}+\frac{m_\rho^2}{2}\boldsymbol{\rho}^{\mu}\cdot\boldsymbol{\rho}_{\mu}-\frac{1}{4}\omega^{\mu\nu}\omega_{\mu\nu}+\frac{m_\omega^2}{2}\omega^{\mu}\omega_{\mu}\\&+\frac{1}{4}f^2\mathrm{Tr}(\partial_\mu U\partial^\mu U^\dagger)+\frac{1}{4}m_\pi^2 f^2\mathrm{Tr}(U+U^\dagger-2)\\&+\frac{1}{2}(\partial_\mu\sigma\partial^\mu\sigma-m_\sigma^2\sigma^2)+\frac{1}{2}(\partial_\mu\boldsymbol{\delta}\cdot\partial^\mu\boldsymbol{\delta}-m_\delta^2\boldsymbol{\delta}^2)\\&+\frac{1}{2}(\partial_\mu\eta\partial^\mu\eta-m_\eta^2\eta^2)+\overline{\psi'}[\gamma^\mu(i\partial_\mu-g_\rho\boldsymbol{\rho}_\mu\cdot\boldsymbol{\tau}-g_\omega\omega_\mu)\\&-U(M+g_\sigma\sigma+g_\delta\boldsymbol{\delta}\cdot\boldsymbol{\tau}+ig_\eta\gamma_5\eta)]\psi',\end{aligned}\tag{1}$$

where the bare masses of the nucleon and the mesons are given by M and m_α where $\alpha=\pi,\eta,\sigma,\delta,\rho,\omega$. We have defined $V^{\mu\nu}\equiv\partial^\mu V^\nu-\partial^\nu V^\mu$ for $V=\rho,\omega$. The notation ψ' indicates a dynamic nucleon field which differs from the free nucleon field, as discussed in Sec. II C 2. The unitary matrix U can be chosen to have one of the three forms U_i:

$$U_1\equiv e^{i\gamma_5\boldsymbol{\tau}\cdot\boldsymbol{\pi}/f},\quad U_2\equiv\frac{1+i\gamma_5\boldsymbol{\tau}\cdot\boldsymbol{\pi}/2f}{1-i\gamma_5\boldsymbol{\tau}\cdot\boldsymbol{\pi}/2f},$$

$$U_3\equiv\sqrt{1-\pi^2/f^2}+i\gamma_5\boldsymbol{\tau}\cdot\boldsymbol{\pi}/f,\tag{2}$$

which correspond to different definitions of the fields. Each of these definitions can be expanded to give

$$U=1+i\gamma_5\frac{\boldsymbol{\tau}\cdot\boldsymbol{\pi}}{f}-\frac{\pi^2}{2f^2}+O\left(\frac{\pi^3}{f^3}\right).\tag{3}$$

In this work, we consider at most two-meson-exchange potentials, so we consider U to be defined by Eq. (3).

In the limit where $m_\pi\to 0$, this Lagrangian, is invariant under the chiral transformation

$$\psi'\to e^{i\gamma_5\boldsymbol{\tau}\cdot\boldsymbol{\alpha}}\psi',\quad U\to e^{-i\gamma_5\boldsymbol{\tau}\cdot\boldsymbol{\alpha}}Ue^{-i\gamma_5\boldsymbol{\tau}\cdot\boldsymbol{\alpha}}.\tag{4}$$

In this model the other mesons are not affected by the transformation because they are not chiral partners of the pion. This is in contrast to the Lagrangian given in Refs. [6,28], where the mass and scalar interaction terms of the nucleon were written as $MU+g_s\phi$ instead of $U(M+g_s\phi)$.

B. Noninteracting nucleon-nucleon theory

The light-front Hamiltonian is derived from this Lagrangian using the same approach used in Refs. [6,19,20,29–32]. The basic idea is to write the light-front Hamiltonian (P^-) as the sum of a free, noninteracting part and a term containing the interactions. We consider the free part first.

1. Free field expansions

The solutions for the free fields are similar to those obtained by using equal-time dynamics. In fact, the solutions are formally related by a change of variable, and so the most obvious difference between the two is due to the Jacobian. The field equations have the general form (when Lorentz, spinor, and isospin indices are suppressed) of

$$\alpha(x)=\int\frac{d^2k_\perp dk^+\theta(k^+)}{(2\pi)^{3/2}\sqrt{2k^+}}[a_\alpha(\boldsymbol{k})e^{-ik^\mu x_\mu}+a_\alpha^\dagger(\boldsymbol{k})e^{+ik^\mu x_\mu}],\tag{5}$$

where $\alpha=\pi,\eta,\sigma,\delta,\rho,\omega,\psi$. Note that in the exponentials

$$k^\mu x_\mu=\frac{1}{2}(k^+x^-+k^-x^+)-\boldsymbol{k}_\perp\cdot\boldsymbol{x}_\perp.\tag{6}$$

The solutions for all the mesons and the nucleon field are given in Ref. [33]. The most general of the commutation relations is

$$[a_{\alpha,i}(\boldsymbol{k},s),a_{\beta,j}^\dagger(\boldsymbol{k}',s')]=\delta_{\alpha,\beta}\delta_{i,j}\delta_{s,s'}\delta^{(2,+)}(\boldsymbol{k}-\boldsymbol{k}'),\tag{7}$$

where α, i, and s denote the meson type, isospin, and spin. The anticommutation relations for the nucleon operators are

$$\begin{aligned}\{b(\boldsymbol{k},\lambda),b^\dagger(\boldsymbol{k}',\lambda')\}&=\{d(\boldsymbol{k},\lambda),d^\dagger(\boldsymbol{k}',\lambda')\}\\&=\delta_{\lambda,\lambda'}\delta^{(2,+)}(\boldsymbol{k}-\boldsymbol{k}').\end{aligned}\tag{8}$$

All other (anticommutation relations vanish. The spinors are normalized so that $\overline{u}(\boldsymbol{p},\lambda')u(\boldsymbol{p},\lambda)=\delta_{\lambda'\lambda}$. For more information on the definition of the spinors, see the Appendix.

2. Noninteracting Hamiltonians

The general form of the noninteracting Hamiltonian for each meson is

$$P_0^-(\alpha)=\int d^2k_\perp dk^+\theta(k^+)a_\alpha^\dagger(\boldsymbol{k})a_\alpha(\boldsymbol{k})\frac{k_\perp^2+m_\alpha^2}{k^+}.\tag{9}$$

For the vector mesons (ρ and ω), there is an implicit sum over the meson spins. Explicitly, this means that for vector mesons $a_V^\dagger(\boldsymbol{k})a_V(\boldsymbol{k})\to\Sigma_{s=1,3}a_V^\dagger(\boldsymbol{k},s)a_V(\boldsymbol{k},s)$. Likewise, the sum over the isospin of the isovector mesons (π, δ, and ρ) is implicit. The sum over isospin can be made explicit by writing $a_I^\dagger(\boldsymbol{k})a_I(\boldsymbol{k})\to\Sigma_{i=1,3}a_{I,i}^\dagger(\boldsymbol{k})a_{I,i}(\boldsymbol{k})$. The noninteracting Hamiltonian for the nucleons has a similar form as well,

$$P_0^-(\psi)=\int d^2k_\perp dk^+\theta(k^+)\Bigg[\sum_{\lambda=+,-} b^\dagger(\boldsymbol{k},\lambda)b(\boldsymbol{k},\lambda) + d^\dagger(\boldsymbol{k},\lambda)d(\boldsymbol{k},\lambda)\Bigg]\frac{k_\perp^2+M^2}{k^+}. \tag{10}$$

These equations are what one expects, since a free particle with momenta $k_\perp$ and k^+ has light-front energy $k^-=(k_\perp^2+m^2)/k^+$.

C. Interacting nucleon-nucleon theory

The interaction Hamiltonians are derived from the Lagrangian in Eq. (1) using standard techniques [19,20]. However, there are some additional complications due to the structure of the interactions.

One complication is that the chiral coupling of the pion field to the nucleons through the U matrix generates vertices with any number of pions. We simply expand the U matrix in powers of $1/f$ and consider the interaction Hamiltonians order by order.

Another complication is due to the fact that both the vector mesons and the fermions have components which depend on other components of the field [6,34–37]. Vector meson fields have four components, but only three degrees of freedom. Likewise, fermion fields have four spinor components, but only two degrees of freedom. When the dependent components are expressed explicitly in terms of the independent components, we obtain new (effective) interaction Hamiltonians for instantaneous vector mesons and fermions. A complete derivation is given by Miller in Ref. [6] and earlier workers cited therein. We illustrate only the main points of the derivation here.

1. Expanding the pion interaction

We start by expanding U in a Taylor series in powers of $1/f$, after which the derivation of the one-meson-interaction Hamiltonian $P'^-_{I,1}$ is straightforward. (The prime indicates that it is in terms of ψ', not ψ. We derive the expressions for $P^-_{I,1}$ in Sec. II C 2.) The result is

$$P^-_{I,1}=\sum_{\alpha=\pi,\eta,\sigma,\delta,\rho,\omega}\int d^2x_\perp dx^-\,\overline{\psi}'(x)g_\alpha\Gamma_\alpha T_\alpha\Phi_\alpha(x)\psi'(x), \tag{11}$$

where we have defined a dimensionless coupling constant $g_\pi\equiv M/f$, denoted the meson fields by Φ_α, and defined

$$\Gamma_\alpha=\begin{cases} i\gamma^5 & \text{if } \alpha \text{ is a pseudoscalar meson } (\pi,\eta),\\ 1 & \text{if } \alpha \text{ is a scalar meson } (\delta,\sigma),\\ \gamma^\mu & \text{if } \alpha \text{ is a vector meson } (\rho,\omega),\end{cases} \tag{12}$$

$$T_\alpha=\begin{cases} \tau_i & \text{if } \alpha \text{ is an isovector meson } (\pi,\delta,\rho),\\ 1 & \text{if } \alpha \text{ is an isoscalar meson } (\eta,\sigma,\omega).\end{cases} \tag{13}$$

In Eq. (11), the appropriate sums over the meson indices are implicit.

The two-meson-interaction Hamiltonian $P'^-_{I,2c}$, which arises from chiral symmetry, has the form

$$P'^-_{I,2c}=\sum_{\alpha=\pi,\eta,\sigma,\delta}\frac{g_\pi g_\alpha}{M}s_\alpha\int d^2x_\perp dx^-\,\overline{\psi}'(x)[\Gamma_\pi T_\pi\Phi_\pi(x)]\times[\Gamma_\alpha T_\alpha\Phi_\alpha(x)]\psi'(x), \tag{14}$$

where s_α is a symmetry factor, equal to $1/2$ when $\alpha=\pi$, and 1 otherwise. When the contact interaction is used to calculate diagrams, an additional factor is picked up for the $\pi\pi$ contact term (due to indistinguishability) which cancels the symmetry factor s_π. Note that this contact interaction involves only scalar and pseudoscalar mesons.

2. Elimination of dependent fermion components

We are now ready to express the dependent components of ψ' in terms of the independent components, and address the problem of instantaneous nucleons. The generation of instantaneous interactions is a general feature of theories with interacting fermions in light-front dynamics where the front has a fixed orientation. Because this is general, we use a simplified model to demonstrate how instantaneous nucleons arise. In particular, we want to postpone the discussion of the complication that the vector mesons introduce until the next section. To this end, we choose to remove all mesons except the σ from the Lagrangian given in Eq. (1). (The σ is chosen since it has the simplest coupling to the nucleon.) The equation of motion for the nucleons is then

$$i\partial\!\!\!/\psi'=(M+g_\sigma\sigma)\psi'. \tag{15}$$

We split Eq. (15) into two equations by applying the projection operators $\Lambda_\pm$, which are defined in the Appendix.

$$i\partial^-\psi'_+=[\boldsymbol{\alpha}_\perp\cdot\boldsymbol{p}_\perp+\beta(M+g_\sigma\sigma)]\psi'_-, \tag{16}$$

$$i\partial^+\psi'_-=[\boldsymbol{\alpha}_\perp\cdot\boldsymbol{p}_\perp+\beta(M+g_\sigma\sigma)]\psi'_+, \tag{17}$$

where $\psi'_\pm=\Lambda_\pm\psi'$. This split is useful because in Eq. (15) all four components of the nucleon field are interrelated, while in Eqs. (16) and (17) the two components of ψ'_+ are related to the two components of ψ'_-, and vice versa.

We must choose which components, ψ'_+ or ψ'_-, are the independent ones. First, notice that Eq. (16) involves ∂^-, a dynamic operator in light-front dynamics. Equations that involve dynamic operators should be avoided, because anything that involves the interaction is complicated. We choose Eq. (17) to avoid that complication and relate the components of ψ. Second, to keep the relation as simple as possible, we do not attempt to invert the spinor matrix on the right side of Eq. (17). Requiring that the equation for the dependent components be both a kinematic equation and simple equation forces us to choose ψ'_+ as the independent components. The dependent components, ψ'_-, are defined by

$$\psi'_-=\frac{1}{p^+}[\boldsymbol{\alpha}_\perp\cdot\boldsymbol{p}_\perp+\beta(M+g_\sigma\sigma)]\psi'_+. \tag{18}$$

The dependent components consist of a noninteracting part and an interacting part while the independent components are noninteracting by definition. Thus we find

$$\psi' = \psi + \xi, \tag{19}$$

where interacting part is

$$\xi = \frac{\gamma^+}{2p^+} g_\sigma \sigma \psi. \tag{20}$$

This allows us to write

$$\psi' = \psi + \frac{\gamma^+}{2p^+} (g_\sigma \sigma) \psi. \tag{21}$$

Plugging Eq. (21) into Eq. (11) and removing all mesons except the σ meson, we obtain

$$P'^-_{I,1} = P^-_{I,1} + P^-_{I,2}, \tag{22}$$

$$P^-_{I,1} = \int d^2x_\perp dx^- \overline{\psi}(x) g_\sigma \sigma(x) \psi(x), \tag{23}$$

$$P^-_{I,2} = 2 \int d^2x_\perp dx^- \overline{\psi}(x) \left[g_\sigma \sigma(x) \frac{\gamma^+}{2p^+} g_\sigma \sigma(x) \right] \psi(x). \tag{24}$$

We interpret the $\gamma^+/2p^+$ factor as a type of nucleon propagator that joins any two meson interactions. Because this propagator does not allow for an energy denominator (as it is already between two potentials), $\gamma^+/2p^+$ is called an *instantaneous* propagator. Thus, when constructing the diagrams for the light-front potentials, we must also include instantaneous propagators for the nucleons in addition to the usual propagators.

3. Elimination of dependent vector meson components

Like the nucleons, the vector mesons have a dependent component that contains interactions and must be eliminated. This process is complicated somewhat by the fact that the dependent nucleon components must be eliminated at the same time. The salient points of the combined elimination of the dependent nucleon and vector meson components are discussed in detail by Miller [6].

The result is that the vector meson field must be redefined and an instantaneous vector meson propagator is generated in addition to an instantaneous nucleon propagator. However, when the nucleon-nucleon potential is calculated, the redefinition of the vector meson field exactly cancels the contribution of the instantaneous vector meson. The result is that the potentials can formally be calculated using the original vector meson field.

In this work, we use that result to simplify our derivations of nucleon-nucleon potentials by formally using the naive form of the vector meson field. Thus, we find an interaction Hamiltonian similar to the one shown in Eq. (24),

$$P'^-_{I,1} = P^-_{I,1} + P^-_{I,2}, \tag{25}$$

$$P^-_{I,1} = \sum_{\alpha=\pi,\eta,\sigma,\delta,\rho,\omega} \int d^2x_\perp dx^- \overline{\psi}(x) g_\alpha \Gamma_\alpha T_\alpha \Phi_\alpha(x) \psi(x), \tag{26}$$

$$P^-_{I,2} = \sum_{\alpha_1,\alpha_2=\pi,\eta,\sigma,\delta,\rho,\omega} \int d^2x_\perp dx^- \overline{\psi}(x) \times [g_{\alpha_1} \Gamma_{\alpha_1} T_{\alpha_1} \Phi_{\alpha_1}(x)] \frac{\gamma^+}{2p^+} \times [g_{\alpha_2} \Gamma_{\alpha_2} T_{\alpha_2} \Phi_{\alpha_2}(x)] \psi(x). \tag{27}$$

We may continue to interpret $\gamma^+/2p^+$ as an instantaneous nucleon propagator, since the derivation in Ref. [6] makes it clear that the potential vanishes when there are two adjacent instantaneous propagators. In Refs. [6,21], the coupling of the vector mesons in the equations equivalent to Eq. (27) has the wrong sign; the sign of coupling of the mesons in Eq. (27) must be the same as in Eq. (26).

In principle the same prescription must be applied to the contact interaction, although to the order of two mesons, this simply removes the primes. We find that

$$P^-_{I,2c} = \sum_{\alpha=\pi,\eta,\sigma,\delta} \frac{s_\alpha}{M} \int d^2x_\perp dx^- \overline{\psi}(x) [g_\pi \Gamma_\pi T_\pi \Phi_\pi(x)] \times [g_\alpha \Gamma_\alpha T_\alpha \Phi_\alpha(x)] \psi(x). \tag{28}$$

The forms of $P^-_{I,2c}$ and $P^-_{I,2}$ are very similar. In fact, we can obtain $P^-_{I,2c}$ from $P^-_{I,2}$ by making the following changes:

(1) Replace $\gamma^+/2p^+$ with s_α/M.
(2) Replace α_1 with π.
(3) Restrict the sum on α_2 to $\pi, \eta, \sigma, \delta$.

4. Interaction Hamiltonians in momentum space

To derive interaction Hamiltonians in momentum space, we examine the matrix element of the interaction Hamiltonians P^-_I between single nucleon initial and final states. We find that the one-meson interaction Hamiltonian can be written as

$$P^-_{I,1}(f,i) = \sum_{\alpha=\pi,\eta,\sigma,\delta,\rho,\omega} g_\alpha 2M \frac{\overline{u}(\boldsymbol{k}_f, \lambda_f) \Gamma_\alpha u(\boldsymbol{k}_i, \lambda_i)}{\sqrt{2(2\pi)^3} \sqrt{k_f^+ k_i^+ q^+}} \times \chi^\dagger_{\tau_f} T_\alpha \chi_{\tau_i} [a_\alpha(\boldsymbol{q}) \theta(k_f^+ - k_i^+) + a^\dagger_\alpha(\boldsymbol{q}) \theta(k_i^+ - k_f^+)] F_\alpha(\boldsymbol{q}). \tag{29}$$

where $\boldsymbol{q} = \{(|k_f^+ - k_i^+|, \mathrm{sgn}(k_f^+ - k_i^+)(\boldsymbol{k}_{f\perp} - \boldsymbol{k}_{i\perp})\}$. The meson-nucleon form factor F_α phenomenologically accounts for the fact that the mesons and nucleons are composite objects. The exact form we use for F_α is given in a later section.

Next we consider the two-meson interactions. Plugging the field definitions into the definition of the interaction with the instantaneous propagator, given by Eq. (27), yields

$$P^-_{I,2}(f,i) = \sum_{\alpha_1,\alpha_2=\pi,\eta,\sigma,\delta,\rho,\omega} g_{\alpha_1} g_{\alpha_2} \times 2M \frac{\bar{u}(\boldsymbol{k}_f,\lambda_f)\Gamma_{\alpha_2}\gamma^+\Gamma_{\alpha_1}u(\boldsymbol{k}_i,\lambda_i)}{2(2\pi)^3\sqrt{k_f^+ k_i^+}} \times[\chi^\dagger_{\tau_f} T_{\alpha_2} T_{\alpha_1}\chi_{\tau_i}] \int \frac{d^2k_{m\perp}dk_m^+\theta(k_m^+)}{2k_m^+\sqrt{q_1^+ q_2^+}} \times[a_{\alpha_2}(k_f-k_m)\theta(k_f^+-k_m^+) + a^\dagger_{\alpha_2}(k_m-k_f)\theta(k_m^+-k_f^+)]F_{\alpha_2}(\boldsymbol{q}_2) \times[a_{\alpha_1}(k_m-k_i)\theta(k_m^+-k_i^+) + a^\dagger_{\alpha_1}(k_i-k_m)\theta(k_i^+-k_m^+)]F_{\alpha_1}(\boldsymbol{q}_1). \quad (30)$$

Note that the momenta q_1 and q_2 are implicitly functions of the momenta k_f, k_m, and k_i. The contact interaction given by Eq. (28) in momentum space can be obtained from Eq. (30) by replacing $\theta(p^+)\gamma^+/2p^+$ with s_α/M and restricting the allowed values of the α's to be consistent with Eq. (28).

D. Feynman rules for nucleon-nucleon potentials

Now that we have the one-meson-exchange and two-meson-exchanges expressed in momentum space, we are now ready to write out the Feynman rules for diagrams in our model. We denote a ''normal'' nucleon propagator by a solid line with an arrow, an instantaneous nucleon propagator by a solid line with a stroke across it, mesons of all types by a dashed line, and energy denominator terms by a vertical, light, dotted line. For simplicity, we consider the only diagrams where a meson emitted by one nucleon is absorbed by the other nucleon. We follow the approach outlined in Ref. [20] to derive the rules:

(1) Overall factor of

$$\frac{4M^2\delta^{\perp,+}(P_f-P_i)}{2(2\pi)^3\sqrt{k_{1f}^+k_{2f}^+k_{1i}^+k_{2i}^+}}.$$

(2) Conserve $\boldsymbol{p}_\perp$ and p^+ momentum.

(3) Factor of $\theta(q_i)/q_i$ for each internal line, including any instantaneous nucleon lines.

(4) Factor of $1/(P^- - \Sigma_i q_i^-)$ for each energy denominator.

(5) Each meson connects the two nucleons, and each end of a meson line has a factor of $g_\alpha\Gamma_\alpha T_\alpha F_\alpha(q)$. The indices of the isospin factors on each end of the meson are contracted together. The Lorentz indices of the gamma matrices are contracted with $-g^{\mu\nu}$ for the vector mesons.

(6) For each contact vertex, multiply by a factor of $1/M$. If the vertex is a $\pi-\pi$ vertex, replace the $T_\pi T_\pi = \tau_i\tau_j$ with $\delta_{i,j}$.

(7) Factor of $(\not{k}+M)/2M = \Sigma_\lambda u(k,\lambda)\bar{u}(k,\lambda)$ for each propagating nucleon and $\gamma^+/2$ for an instantaneous nucleon.

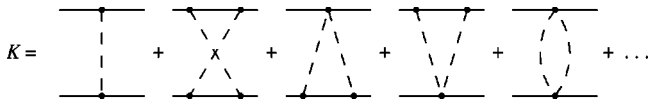

FIG. 1. The first several terms of the full kernel for the Bethe-Salpeter equation of the nuclear model with chiral symmetry.

(8) Integrate with

$$4M^2\int\frac{d^2k_\perp dk^+}{2(2\pi)^3}$$

over any internal momentum loops.

(9) Put the spinor factors for nucleon 1 and 2 between $\bar{u}u$'s and the isospin factors between the initial and final state isospin.

E. Nucleon-nucleon potentials

The meson exchange potentials have the same basic form as in Refs. [19,20]; however, we must include the contact interaction and instantaneous nucleon propagators for the nuclear model used here. First, we discuss how to include the contact diagrams from the standpoint of the Bethe-Salpeter equation, then we begin to calculate the light-front potentials.

1. The Bethe-Salpeter equation and chiral symmetry

The kernel of the Bethe-Salpeter equation [38–42] for this nuclear model is richer than the one presented in Refs. [20] for the Wick-Cutkosky model. This is due mainly to the presence of the contact interactions which are generated by the chirally invariant coupling of the pion to the nucleon. Several of the lowest-order pieces of the full kernel K are shown in Fig. 1. (Note that for Feynman diagrams, it is useful to combine the ''normal'' nucleon propagator with the instantaneous nucleon propagator [43–45], and denote the combination with a solid line.) Each of these Feynman diagrams is covariant. This means that we may choose any of the diagrams from K to construct a new kernel K', and the infinite series of potential diagrams ''physically equivalent'' to K' will also be covariant [19,20]. The equivalence permits us to apply arguments about the symmetries of the Bethe-Salpeter equation to light-front dynamics [43–45]. In practice, this covariance means that when deciding which two-meson-exchange potentials to include for calculating the deuteron wave function, we may neglect the crossed diagrams. Although including only the box and contact two-meson-exchange diagrams may affect the exact binding energy calculated, we should find a partial restoration of rotational invariance. We reiterate that the focus of this work is on understanding the effects of the breaking of rotational invariance and how to restore it; our goal is not precise agreement with experimental results.

We also want to keep the potentials chirally symmetric as well. Whereas Lorentz symmetry is maintained by using a kernel with any Feynman diagrams (with potentially arbitrary coefficients), chiral symmetry relates the strength of the $\pi\pi$ contact interaction to the strength of the pion-nucleon coupling.

In Ref. [46], we showed that chiral symmetry can have a significant effect on calculations. The contact potentials cancel strongly with both the iterated box potentials and the crossed potentials, reducing the strength of the total two-pion-exchange potential and leading to more stable results. We also found that approximate chiral symmetry can be incorporated for two-meson-exchange box graphs by adding the contact graphs weighted with a factor of $M/2(M+m_\pi)$. This factor is not needed for one meson exchange graphs.

2. OME and TME potentials

The potentials we consider connect an initial state with two nucleons to a final state with two nucleons, and the intermediate-state mesons are each emitted and absorbed by different nucleons. These restrictions, together with the fact that in light-front dynamics massive particles cannot be created from the vacuum, means there are two nontrivial OME, as shown in Fig. 2. As discussed in the previous section, the

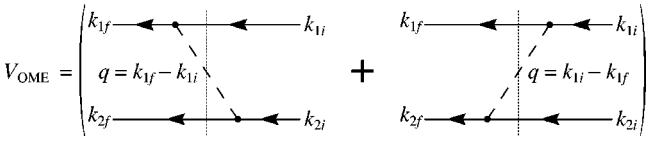

FIG. 2. The two diagrams which contribute to the OME potential for each meson.

TME potentials can be classified into three groups. The Feynman rules derived in the previous section are used to derive the potential for these diagrams. We factor out an overall factor of

$$\frac{4M^2\delta(k_{1f}+k_{2f}-k_{1i}-k_{2i})}{2\sqrt{k_{1f}^+k_{1i}^+k_{2f}^+k_{2i}^+}}$$

that is common to all the two-nucleon potentials and suppress it from now on. Then we get

$$V_{\mathrm{OME},\alpha}=\frac{g_\alpha^2 \boldsymbol{T}_{\alpha,1}\cdot\boldsymbol{T}_{\alpha,2}}{(2\pi)^3}\overline{u}(\boldsymbol{k}_{1f},\lambda_{1f})\Gamma_\alpha u(\boldsymbol{k}_{1i},\lambda_{1i})\overline{u}(\boldsymbol{k}_{2f},\lambda_{2f})\Gamma_\alpha u(\boldsymbol{k}_{2i},\lambda_{2i})F_\alpha^2(\boldsymbol{q})$$
$$\times\left[\frac{\theta(k_{1f}^+-k_{1i}^+)}{(k_{1f}^+-k_{1i}^+)(P^- -k_{1i}^- -k_{2f}^-)-m_\alpha^2-(k_{1i,\perp}-k_{1f,\perp})^2}+\frac{\theta(k_{1i}^+-k_{1f}^+)}{(k_{1i}^+-k_{1f}^+)(P^- -k_{1f}^- -k_{2i}^-)-m_\alpha^2-(k_{1i,\perp}-k_{1f,\perp})^2}\right]. \tag{31}$$

In the scattering regime ($P^-=k_{1f}^-+k_{2f}^-=k_{1i}^-+k_{2i}^-$), Eq. (31) agrees with Eq. (4.7) in Ref. [6], after taking into account the difference in spinor normalization (we use $\overline{u}u=1$).

Now we consider the precise form to use for the meson-nucleon form factor. We assume that it has a *n*-pole form [23], so that the denominator of the meson-nucleon form factor has the same form as the denominator of the potential in the scattering regime. In particular, Λ_α plays the role of m_α for the form factor. For simplicity, we declare that the denominator of the form factor always has the same form of the denominator of the potential. Thus,

$$F_\alpha(\boldsymbol{q})=\left(\frac{\Lambda_\alpha^2-m_\alpha^2}{a-\Lambda_\pi^2+b\cos(\phi_f-\phi_i)}\right)^{n_\alpha}. \tag{32}$$

The TME potentials considered here are the box diagrams, Fig. 3, and the contact diagrams, Fig. 4. We do not consider the crossed diagrams because they are not needed to restore rotational invariance, as discussed in Sec. II E 1. Reference [33] shows that each of the potentials in Figs. 3 and 4 can be written schematically in the following general form:

$$V_{\mathrm{TME}}=\frac{g^4 4M^2T^4}{(2\pi)^3}\int\frac{d^2k_{2m\perp}dk_{2m}^+}{2(2\pi)^3}f(k_{1m}^+,k_{2m}^+,q_f^+,q_i^+)\overline{u}(\boldsymbol{k}_{1f},\lambda_{1f})\Gamma_{\alpha_f}\mathcal{M}_1\Gamma_{\alpha_i}u(\boldsymbol{k}_{1i},\lambda_{1i})\overline{u}(\boldsymbol{k}_{2f},\lambda_{2f})\Gamma_{\alpha_f}\mathcal{M}_2\Gamma_{\alpha_i}u(\boldsymbol{k}_{2i},\lambda_{2i})$$
$$\times[a_f-m_{\alpha_f}^2+b_f\cos(\phi_f-\phi_m)]^{-n_f}F_{\alpha_f}(\boldsymbol{q}_f)^2[a_m+b_{mf}\cos(\phi_f-\phi_m)+b_{mi}\cos(\phi_m-\phi_i)]^{-n_m}$$
$$\times[a_i-m_{\alpha_i}^2+b_i\cos(\phi_m-\phi_i)]^{-n_i}F_{\alpha_i}(\boldsymbol{q}_i)^2. \tag{33}$$

3. Further development of the light-front Schrödinger equation

The potentials derived here possess a high degree of symmetry. To solve the light-front Schrödinger equation efficiently, these symmetries should be explicitly exploited, as was done in Refs. [19,20]. In addition, there are additional symmetries due to the conservation of nucleon helicity and invariance under time reversal [23].

We follow Machleidt's approach for taking advantage of the symmetry of rotationally invariant potentials with helicity [24]. However, since the light-front potentials derived

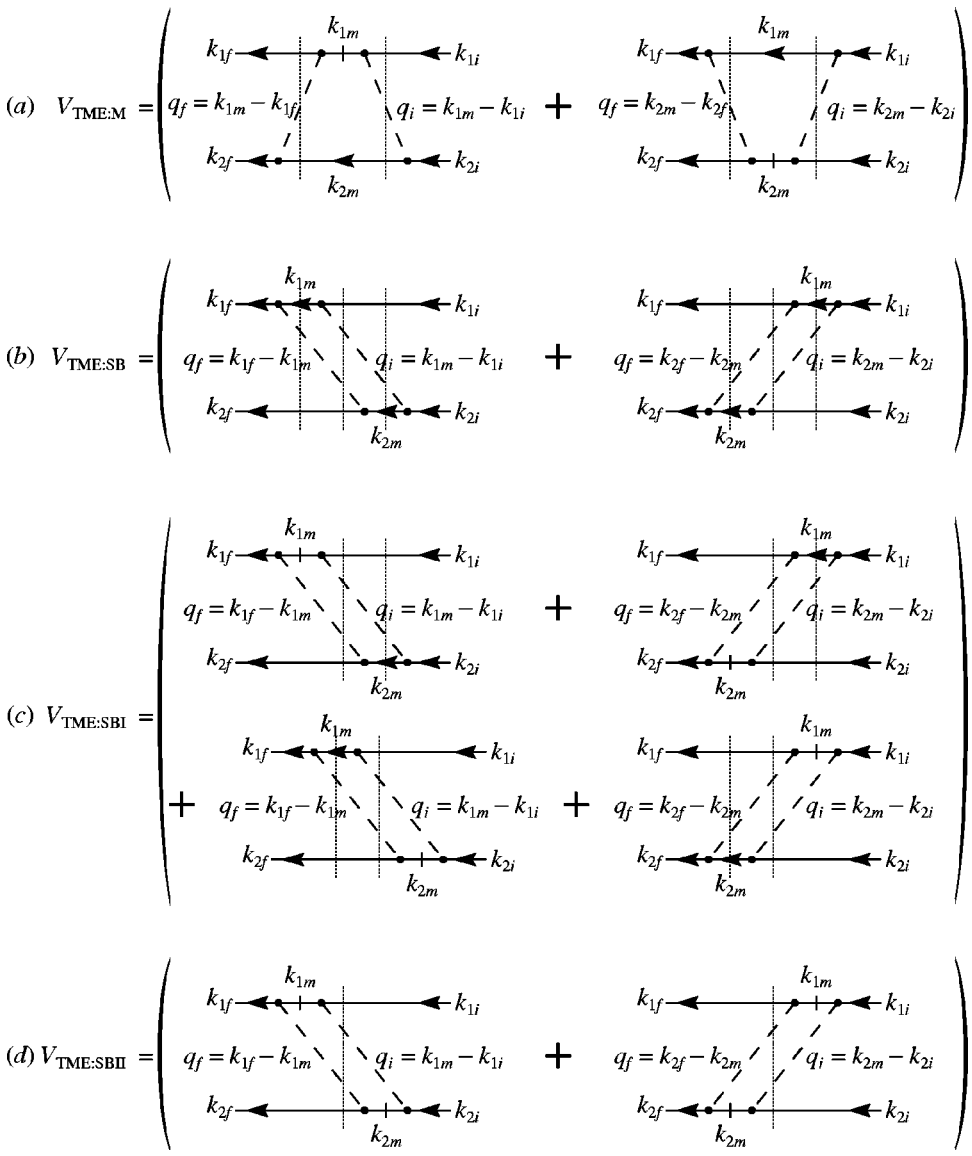

FIG. 3. The TME potentials for (a) $V_{\mathrm{TME:M}}$ (the Mesa potential), (b) $V_{\mathrm{TME:SB}}$ (the stretched box potential), (c) $V_{\mathrm{TME:SBI}}$ (the stretched instantaneous potential), and (d) $V_{\mathrm{TME:SBII}}$ (the stretched double instantaneous potential). Note that the graphs on the right side are obtained from the graphs on the left side by $1 \leftrightarrow 2$.

here do not have full rotational invariance, the approach must be modified. The symmetry properties of helicity matrix elements are rederived in Ref. [33] without assuming full rotational invariance. These results allow a modified version of Machleidt's approach to be combined with the exploitation of parity (using the transformation from light-front coordinates to equal-time coordinates) discussed in Refs. [19,20]. In particular, the potentials are initially calculated in the $|p_{\mathrm{ET}},\theta,M,\lambda_1,\lambda_2\rangle$ basis, although the relations in Ref. [33] are used to transform to the $|p_{\mathrm{ET}},J,M,L,S\rangle$ basis to solve for the wave functions. In general, the potentials connect states with different values of J. Once the symmetries have been explicitly expressed, we can discretize the Schrödinger equation as done in Ref. [20,33]. We can choose which truncation of the light-front nucleon-nucleon (LFNN) potential to use in the Schrödinger equation, however, different truncations of the potential give rise to different wave functions.

Note that the transformations applied to the potential in order to simplify the solution of the wave functions. Once the wave functions are obtained, we may apply the inverse of the transformations to the wave functions to express them in the helicity basis ($|\boldsymbol{p}_\perp,p^+,\lambda_1,\lambda_2\rangle$) or in the light-front spin basis ($|\boldsymbol{p}_\perp,p^+,m_1,m_2\rangle$) [33].

III. FORM FACTORS OF THE DEUTERON

In the previous section, we discussed how to derive several deuteron wave functions for different truncations of the LFNN potential. In this section, we use those wave functions to solve for the matrix elements of the deuteron current operator, which is used to calculate the deuteron electromagnetic and axial form factors.

We outline the covariant theory of the electromagnetic form factors for spin-1 objects, such as the deuteron. Then we recall the features of light-front calculations (including the breaking of rotational invariance) of the form factors. After that, we review the covariant and light-front tools for calculating axial form factors. The formalism is then applied to calculate the electromagnetic and axial currents and form factors for the light-front deuteron wave functions.

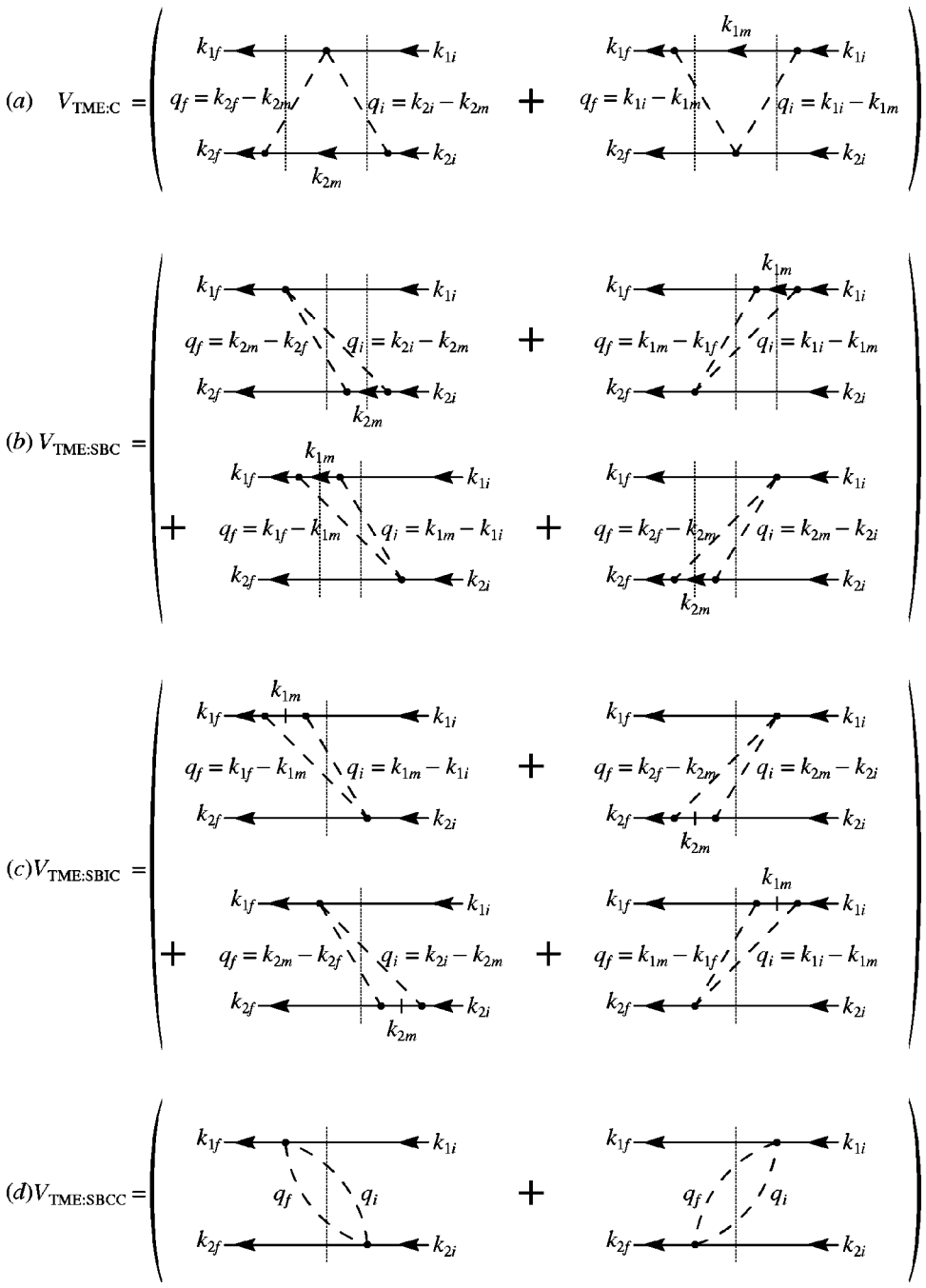

FIG. 4. The TME potentials that include the contact interaction for (a) $V_{\mathrm{TME:C}}$ (the contact potential), (b) $V_{\mathrm{TME:SBC}}$ (the stretched contact potential), (c) $V_{\mathrm{TME:SBIC}}$ (the stretched instantaneous contact potential), and (d) $V_{\mathrm{TME:SBCC}}$ (the stretched double contact potential). Note that the graphs on the right side are obtained from the graphs on the left side by $1 \leftrightarrow 2$.

A. Electromagnetic form factors

1. Covariant theory

In the one-photon-exchange approximation, shown in Fig. 5, the amplitude of the scattering process $ed \rightarrow ed$ is just the contraction of the electron and deuteron current matrix elements, multiplied by the photon propagator,

$$\langle p', \lambda' | j^e_\mu | p, \lambda \rangle \frac{1}{q^2} \langle k', m' | J^\mu_d | k, m \rangle, \tag{34}$$

where j^e_μ is the electron current operator. From Lorentz co-

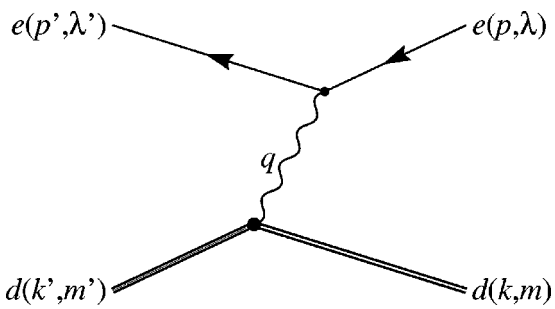

FIG. 5. The Feynman diagram for one-photon-exchange electron-deuteron scattering.

variance, parity invariance, time-reversal invariance, and current conservation [47–51], we infer that the deuteron form factor can be written as

$$\langle k',m'|J_d^\mu|k,m\rangle = -\frac{e}{2M_d}(e^*)^\rho(\boldsymbol{k}',m')J^\mu_{\rho\sigma}e^\sigma(\boldsymbol{k},m), \tag{35}$$

where the spin-1 polarization vectors satisfy the usual relations and the operator $J^\mu_{\rho\sigma}$ is given by

$$J^\mu_{\rho\sigma}=(k'_\mu+k_\mu)\left[g_{\rho\sigma}F_1(q^2)-\frac{q_\rho q_\sigma}{2M_d^2}F_2(q^2)\right]-I^{\mu\nu}_{\rho\sigma}q_\nu G_1(q^2), \tag{36}$$

where $I^{\mu\nu}_{\rho\sigma}=g^\mu_\rho g^\nu_\sigma - g^\nu_\rho g^\mu_\sigma$ is the generator of infinitesimal Lorentz transformations, $q=k'-k$, and F_1, F_2, and G_1 are functions of q^2, the invariant mass of the photon.

The F_1, F_2, and G_1 form factors are related to the deuteron charge, magnetic, and quadrapole form factors, denoted by F_C, F_M, and F_Q respectively, by [47,49,52]

$$F_C=F_1+\frac{2}{3}\eta[F_1+(1+\eta)F_2-G_1], \tag{37}$$

$$F_M=G_1, \tag{38}$$

$$F_Q=F_1+(1+\eta)F_2-G_1, \tag{39}$$

where

$$\eta=\frac{-q^2}{4M_d^2}. \tag{40}$$

Note that since both the initial and final electron and deuteron are on-shell, $-q^2>0$. We define $Q^2=-q^2$. The numerical values of the form factors are determined by using experimentally measured values [50,53,54].

To experimentally determine the deuteron form factors, electron-deuteron cross sections are measured. Unpolarized cross section measurements yield the structure functions A and B, which can be expressed as [50,55]

$$A=F_C^2+\frac{8}{9}\eta^2F_Q^2+\frac{2}{3}\eta F_M^2, \tag{41}$$

$$B=\frac{4}{3}\eta(1+\eta)F_M^2. \tag{42}$$

Polarized cross section measurements yield tensor polarization observables, such as T_{20} [50,51]

$$T_{20}=-\frac{\frac{8}{3}\eta F_C F_Q+\frac{8}{9}\eta^2F_Q^2+\frac{1}{3}\eta F_M^2[1+2(1+\eta)\tan^2(\theta_e/2)]}{\sqrt{2}[A+B\tan^2(\theta_e/2)]}, \tag{43}$$

where θ_e is the angle by which the electron scatters. Data for T_{20} are usually presented for $\theta_e=70°$.

2. Light-front calculation

Light-front dynamics is particularly well suited to calculating form factors. One reason is that the generators of boosts in the one, two, and plus directions are kinematic, so that wave functions calculated with a truncated potential transform correctly under boosts. This feature is especially important for form factors at high momentum transfer, because the wave functions must undergo a large boost.

Another, more subtle, reason for using the light front is that many of the graphs which contribute to the current vanish identically. For example, the three lowest-order graphs for the current are shown in Fig. 6. The double line denotes the deuteron, and the vertex of the deuteron lines and the nucleon lines represents the deuteron wave function. The graph labeled (a) does not vanish and is calculated in Sec. III A 5. Figure 6(b) vanishes in light-front dynamics. To see why, we first note three facts: the plus component of each particle in light-front dynamics is nonnegative (for massive particles it must be positive), the plus component of the momentum is conserved, and the plus momentum of the vacuum is zero. Combining these facts, we find that any vertex which has particles on one side and vacuum on the other must vanish. In other words, the vacuum is trivially empty, and no graphs couple to it.

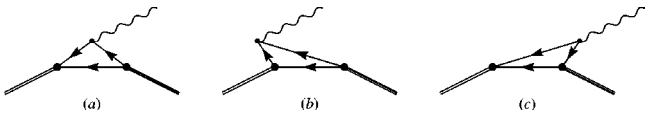

FIG. 6. The lowest-order time-ordered graphs that contribute to the deuteron current matrix element.

For Fig. 6(c), the coupling of the photon to the nucleon varies as $\bar{u}_{\rm LF}\gamma^\mu v_{\rm LF}$, where the light-front spinors are defined in the Appendix. For $\mu=+$, this matrix element is suppressed maximally, and thus J^+ is the ''good'' component of the current [11,13,56]. We calculate only J^+, since it is the most stable.

We do not consider the contribution of higher-order graphs to the deuteron current, such as graphs where the photon couples to a meson or a nucleon while a meson is present. The omission of the meson-exchange currents is justified only if the current of a composite particle factorizes in

the impulse approximation. We start by writing the total current $J_T^\mu(q)$ as

$$J_T^\mu(q)=\sum_i F_i(q)J_i^\mu(q), \tag{44}$$

where the sum runs over all constituent particles, $F_i(q)$ is a form factor of particle i, and J_i is independent of form factors. If the electromagnetic form factors of the meson and the nucleon are independent, then each J_i must have the same symmetry properties as J_T. Thus, omitting the meson exchange currents does not affect the rotational properties of the current although it does affect the overall values of the deuteron form factors. This is acceptable since we are only concerned with the rotational properties in this work, not in the detailed results.

The neglect of the graphs where the photon couples to a nucleon while a meson is present is a sign that the calculation is not complete. Indeed, the deuteron current shown in Fig. 6(a) is not formally conserved [55]. But current conservation is a necessary consequence of a complete calculation in this model. To construct the conserved current operator associated with a given wave function, the current must include diagrams that are related to the potential used to calculate the wave function. We expect that these diagrams are small since they contain meson propagators.

3. Symmetries of the electromagnetic current

Symmetries relate the components of $\langle k',m'|J^+(q)|k,m\rangle$. In particular, the generators of boosts in the plane perpendicular to the z axis, boosts in the plus direction, and rotations about the z axis are kinematic. In addition, we will find how the states and the current operator transforms under kinematic parity and time reversal.

The kinematic generators allow us to choose which frame to evaluate the current in. We choose the frame [11] where $q^+=q^-=q_\perp^y=0$ and $q_\perp^x=Q$. We also choose the plus momentum of the deuteron to be M_d, since M_d is the value of the plus momentum in deuteron's rest frame. To simplify the notation, we define the light-front spinor matrix elements of J^+ as

$$I^+_{m',m}(Q)=\left\langle \frac{\boldsymbol{q}_\perp}{2},m'\middle|J^+(Q)\middle|-\frac{\boldsymbol{q}_\perp}{2},m\right\rangle. \tag{45}$$

This quantity is represented by $I_{m'm}$, not $J_{m'm}$, because $J_{m'm}$ is used to represent the matrix elements of J using the instant-form spin basis. The two matrices are related by the Melosh transformation [13,57].

The symmetries dictate that of the nine possible matrix elements of J^+, there are only four independent components. We choose those components to be I^+_{11}, I^+_{10}, I^+_{1-1}, and I^+_{00}. It is helpful to express the matrix elements in a matrix to see the symmetry properties explicitly:

$$I^+_{m',m}=\begin{pmatrix} I^+_{11} & I^+_{10} & I^+_{1-1} \\ -I^+_{10} & I^+_{00} & I^+_{10} \\ I^+_{1-1} & -I^+_{10} & I^+_{11} \end{pmatrix}. \tag{46}$$

4. Rotational invariance and the angular condition

This is as far as we can go with light-front dynamics, but there should be an additional redundancy in our matrix elements. We have derived four independent components, whereas in a fully covariant framework there are only three form factors. The resolution of this conflict is that full rotational invariance imposes an *angular condition* on the light-front matrix elements.

The deviation from the angular condition, which we denote with Δ, is given by [14]

$$\Delta=-I^+_{00}+(1+2\eta)I^+_{11}+I^+_{1-1}-2\sqrt{2\eta}I^+_{10}, \tag{47}$$

where η is defined by Eq. (40). Since Δ vanishes when the deuteron current transforms correctly under rotations, we interpret Δ as a measure of the extent to which the current transforms incorrectly.

The form factors are over determined by the current matrix elements, which means many different relations possible. When Δ is zero, all the relations are equivalent, while a nonzero Δ means that the form factors depend also on which relation is chosen.

Since Δ is nonzero in general, it is important to choose the best relation to obtain the form factor. To do this, we classify the current matrix elements as either ''good'' or ''bad.'' This classification is similar to the one made for choosing which component of the current to use.

In this work we are interested in the overall rotational invariance properties; the choice of how to relate the form factors is simply useful for comparing with other approaches. In that spirit, we consider four different choices [14].

(1) Grach and Kondratyuk (GK) consider I^+_{00} as the bad element [58].

(2) Brodsky and Hiller (BH) use a prescription where I^+_{11} is bad [59].

(3) Frankfurt, Frederico, and Strikman (FFS) use the Cartesian component J^+_{zz} as the bad current [11].

(4) Chung, Polyzou, Coester, and Keister (CCKP) choose the canonical expressions for the form factors in terms of the equal-time current, then use rotations and the Melosh transformation to express the equal-time current matrix elements in terms of the light-front current matrix elements [18,52].

5. Impulse approximation on the light front

We now are ready to relate the deuteron wave function to the current. Inserting a complete set of light-front spinor states into Eq. (45) gives

$$I^{+}_{m',m}(q)=\int d^2p_\perp dp^+ \sum_{m'_1,m_1,m_2} \times 2\bar{u}_{\rm LF}(p^+,\boldsymbol{p}_\perp+\boldsymbol{q}_\perp/2,m'_1) \times J^{+}_{(S)}(\boldsymbol{q}_\perp)u_{\rm LF}(p^+,\boldsymbol{p}_\perp-\boldsymbol{q}_\perp/2,m_1) \times\langle \boldsymbol{q}_\perp/2,m'|p^+,\boldsymbol{p}_\perp+\boldsymbol{q}_\perp/2,m'_1,m_2\rangle 2 \times\langle p^+,\boldsymbol{p}_\perp-\boldsymbol{q}_\perp/2,m_1,m_2|-\boldsymbol{q}_\perp/2,m\rangle, \quad (48)$$

where the light-front spins of particles 1 and 2 are labeled m_1 and m_2, respectively. Because the deuteron is an isoscalar combination of nucleons, the isovector component of the nucleon current does not contribute and the isoscalar nucleon current is the same for both nucleons. This allows us to simply double the isoscalar current of particle 1 instead of using the isoscalar currents of both particle 1 and 2.

To relate this current to the wave functions we calculate, we must boost the deuteron wave functions to the rest frame. The boost that accomplishes this transforms a general light-front vector from $\{k^+,\boldsymbol{k}_\perp\}$ to $\{k^+,\boldsymbol{k}_\perp+x\boldsymbol{q}_\perp/2\}$, where $x=p^+/M_d$ is the Bjorken x variable. Applying this to the deuteron wave function gives

$$\langle \boldsymbol{q}_\perp/2,m|p^+,\boldsymbol{p}_\perp+\boldsymbol{q}_\perp/2,m_1,m_2\rangle =\langle m|p^+,\boldsymbol{p}_\perp+(1-x)\boldsymbol{q}_\perp/2,m_1,m_2\rangle. \quad (49)$$

The deuteron wave functions solved in Sec. II can be used in the right-hand side of Eq. (49). Note that the light-front spin labels are unaffected by the boosts.

6. The nucleon form factors

From Lorentz covariance, parity invariance, and time-reversal invariance [48,49], the isoscalar part of the nucleon current can be expressed as

$$J^{\mu}_{(S)}(q)=\sum_{i=1,2} F^{(S)}_i(q)J^{\mu}_{(iS)}(q), \quad (50)$$

where

$$J^{\mu}_{(1S)}(q)=\gamma^\mu, \quad (51)$$

$$J^{\mu}_{(2S)}(q)=i\frac{\sigma^{\mu\nu}q_\nu}{2M}, \quad (52)$$

and $F^{(S)}_1$ and $F^{(S)}_2$ are the isoscalar Dirac and Pauli form factors, respectively. They are normalized to $F^{(S)}_1(0)=1/2$ and $F^{(S)}_2(0)=(\kappa_p+\kappa_n-1)/2$.

When Eq. (50) is inserted into Eq. (48), we get

$$I^{+}_{m',m}(q)=\sum_{i=1,2} F^{(S)}_i(q)I^{+}_{(i)m',m}(q), \quad (53)$$

where

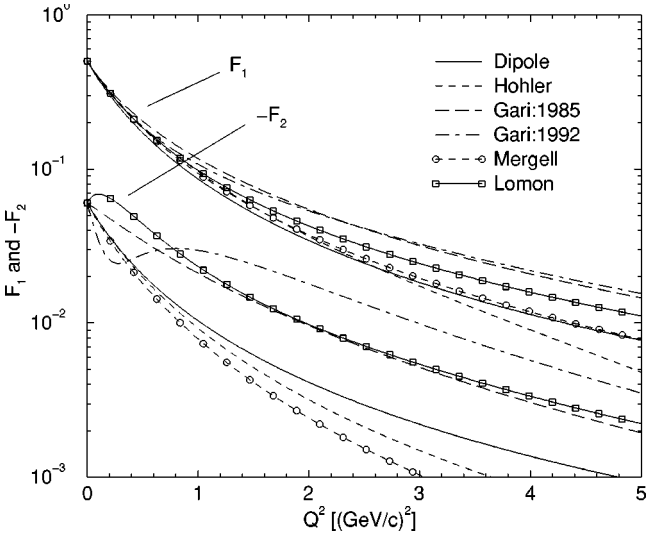

FIG. 7. The F_1 and $-F_2$ isoscalar nucleon form factors for six different models: the dipole model, Hohler, Gari: 1985, Gari: 1992, Mergell, and Lomon.

$$I^{+}_{(i)m',m}(q)=\int d^2p_\perp dp^+ \sum_{m'_1,m_1,m_2} \times 2\bar{u}_{\rm LF}(p^+,\boldsymbol{p}_\perp+\boldsymbol{q}_\perp/2,m'_1) \times J^{+}_{(iS)}(\boldsymbol{q}_\perp)u_{\rm LF}(p^+,\boldsymbol{p}_\perp-\boldsymbol{q}_\perp/2,m_1) \times\langle m'|p^+,\boldsymbol{p}_\perp+(1-x)\boldsymbol{q}_\perp/2,m'_1,m_2\rangle \times\langle p^+,\boldsymbol{p}_\perp-(1-x)\boldsymbol{q}_\perp/2,m_1,m_2|m\rangle, \quad (54)$$

for $i=1,2$. Note that both $J^{+}_{(1)m',m}(q)$ and $J^{+}_{(2)m',m}(q)$ must satisfy the same equations as $J^{+}_{m',m}(q)$ does. In particular, this means that the angular condition applies to $J^{+}_{(1)m',m}(q)$ and $J^{+}_{(2)m',m}(q)$ independently, so we consider the deviation from the angular condition for each.

There are many parametrizations of the isoscalar nucleon form factors $F^{(S)}_1(q)$ and $F^{(S)}_2(q)$. Since the measurement of the electron-nucleon cross section is difficult, the data have large errors and are consistent with several different models of the nucleon form factors. Some of the models representative of those proposed in the literature are: the dipole model, fit 8.2 of Hohler *et al.* [60], Gari and Krümpelmann, 1985 [61], model 3 of Gari and Krümpelmann, 1992 [62,63], best fit for the multiplicative parametrization of Mergell and others [64], and model DR-GK(1) [dispersion relation for Gari Krümpelmann (1)] of Lomon [65]. The $F^{(S)}_1(q)$ and $F^{(S)}_2(q)$ form factors for each of these models are shown in Fig. 7.

We can relate the isovector form factors to G_{Ep}, G_{Mp}, G_{En}, and G_{Mn}, the proton electric, proton magnetic, neutron electric, and neutron magnetic form factors, respectively, with [66]

$$F^{(S)}_1=\frac{G_{Ep}+G_{En}+\tau(G_{Mp}+G_{Mn})}{2(1+\tau)}, \quad (55)$$

$$F^{(S)}_2=\frac{-G_{Ep}-G_{En}+G_{Mp}+G_{Mn}}{2(1+\tau)}, \quad (56)$$

where $\tau \equiv Q^2/4M$. The value of τ is approximately 1 at a momentum transfer of about 5 GeV^2, the upper range of momentum transfers that we consider. Since the overall magnitudes of the form factors are similar at this momentum transfer, it is important to measure each of the form factors with the same accuracy and cover the same range of momentum transfers. Currently, the most poorly known form factor is G_{En}, both in terms of the magnitude of the error and in the number of data points [65].

In Sec. IV B, we will find that for momentum transfers greater than about 2 GeV^2, the spread in the values of the deuteron form factors due to the breaking of rotational invariance on the light front is smaller than the spread in values due to using the various nucleon form factors. It is uncertainty of the nucleon form factors, not the use of the light front, that limits the accuracy of the deuteron form factors at large momentum transfers. Only more accurate measurements of the nucleon form factors, especially G_{En}, will allow for more accurate deuteron form factor calculations.

B. Axial form factors

The formalism used for the axial current and form factor is very similar to that used for the electromagnetic current and form factor. Thus, most of the discussion from the previous section carries over here with only slight modifications. We highlight only the differences.

The derivation of the symmetries of the axial current matrix elements is almost the same as in Sec. III A 2, with the exception that under parity [67] the axial current picks up a negative sign. This means that of the nine possible matrix elements of J_5^+, there are only two independent components. We choose those components to be $I^+_{(5)11}$, and $I^+_{(5)10}$. It is helpful to express the matrix elements in a matrix to see the symmetry properties explicitly.

$$I^+_{(5)m',m} = \begin{pmatrix} I^+_{(5)11} & I^+_{(5)10} & 0 \\ -I^+_{(5)10} & 0 & -I^+_{(5)10} \\ 0 & I^+_{(5)10} & -I^+_{(5)11} \end{pmatrix}. \tag{57}$$

We have derived two independent components, but an analysis of the covariant theory shows that only one deuteron form factor (F_A) contributes for the plus component of the axial current [12]. This implies that the requirement of full rotational invariance imposes an angular condition on the light-front axial current matrix elements. The deviation from the angular condition, denoted by Δ, is given by [12]

$$\Delta = \frac{\sqrt{2\eta}}{2} I^+_{(5)11} - I^+_{(5)10}. \tag{58}$$

Since the deuteron axial form factor is overdetermined by the current matrix elements, we need to classify the current matrix elements as either ''good'' or ''bad'' to eliminate ambiguity. We consider two such choices.

(1) Frankfurt, Frederico, and Strikman (FFS) find that the $J^+_{(5)zz}$ is the bad matrix element [11].

(2) Frederico, Henley, and Miller (FHM) use the behavior of the matrix elements in the nonrelativistic limit to determine that the bad element is $I^+_{(5)10}$ [12].

The current matrix elements are calculated using the nucleon axial current. Since we choose to use $\mu = +$ and work in the frame where $q^+ = 0$, the general form of nucleon axial current reduces to

$$J^+_{(5)n} = \gamma^+ \gamma^5 F^n_A. \tag{59}$$

Since the deuteron axial current has such a simple functional dependence on the nucleon axial form factor, we choose to use the dipole model with the value of the axial mass determined by Liesenfeld *et al.* [68].

IV. RESULTS

A. Deuteron binding energies

The next step towards numerically calculating the bound states for these potentials is to choose the parameters (meson masses, coupling constants, etc.) for the potentials. We consider the full nuclear model where the nucleon-nucleon interaction is mediated by the π, η, ρ, ω, δ, and σ mesons. For numerical work, use the parameters for the light-front nucleon-nucleon (LFNN) potential from the work of Miller and Machleidt [21]. Those parameters were fit for a potential that used a retarded propagator for the energy in the potentials. Since the potentials used in this paper have energy dependent denominators (arising from the elimination of the Fock space components containing mesons or more than two nucleons) the parameters must be modified somewhat. We choose the σ meson coupling constant to be f_σ times the coupling constant given in Ref. [21], and we vary f_σ.

As with all the other deuteron models presented in this paper, the light-front OME potential breaks rotational invariance and causes a mass splitting of the deuteron states with different magnetic quantum numbers. We expect that the splitting will be removed somewhat by including higher-order potentials.

The first step is to determine which two-meson-exchange potentials to use. One choice is to use only the two-pion-exchange potentials, TPE and ncTPE, as defined in the previous section. However, we expect to get better results using the two-meson-exchange diagrams generated by all the available mesons, including the contact diagrams for the pions, which we denote as the two-meson-exchange (TME) potential. In addition, we can also investigate the effect of leaving out the contact potentials for the pions, resulting in the nonchiral two-meson-exchange (ncTME) potential.

We do not include diagrams with a contact interaction between the nucleon, a pion, and another meson. This is because, as mentioned in Sec. II E 1, the infinite series of the box diagrams is rotationally invariant and the contact diagrams are not needed to achieve rotational invariance. Furthermore, they are not required to control the convergence of the series, since there is no strong cancellation between the contact diagram and the instantaneous diagrams.

The first step in analyzing the bound states is to determine what range of f_σ gives reasonable results. We iteratively

TABLE I. The values of f_σ required to give the physical value of the deuteron mass for a given potential and state with $J_z=m$. The percent of the wave function in the D-state and in the $J=1$ state are also shown.

Potential	f_σ			% D state		% $J=1$	
	$m=0$	$m=1$	Diff	$m=0$	$m=1$	$m=0$	$m=1$
OME	1.2407	1.2125	0.0282	2.87	3.55	99.99	99.97
OME +TPE	1.2829	1.2819	0.0010	2.96	3.23	99.99	99.97
OME +TME	1.2968	1.3079	−0.0111	2.95	3.28	99.99	99.96
OME +ncTPE	1.3064	1.3121	−0.0057	2.99	3.16	99.98	99.97
OME +ncTME	1.3198	1.3397	−0.0199	2.98	3.21	99.98	99.96

solve for the binding energy of the deuteron, varying f_σ until the binding energy matches the physical value of the binding energy, for each of the potentials. The results are shown in Table I. We find that a value of f_σ in the range 1.2 to 1.3 will give reasonable results for the binding energy. Note that D-state probability (about 3%) is lower in this model than for the energy-independent light front used in Ref. [21], where a value of 4.5% is found. This is expected since the f_σ is greater than 1 in this model, meaning that the scalar interaction is strengthened relative to the tensor interaction, leading to a decrease in amount of the D state present.

We choose two values of f_σ, one from the low end of the range (1.22) and one from the high end (1.2815) for our investigations. Using two values helps ensure that our results are robust.

First, we examine the bound states for $f_\sigma=1.22$. The results for several different choices of the TME potentials are shown in Table II and the binding energies are plotted in Fig. 8. In addition to the two-meson-exchange potentials mentioned above, we also consider the π-σ plus π-ω mesa potential. The reason for considering this potential is that Carbonell, Desplanques, Karmanov, and Mathiot [69] have shown that it helps restore rotational invariance of the deuteron.

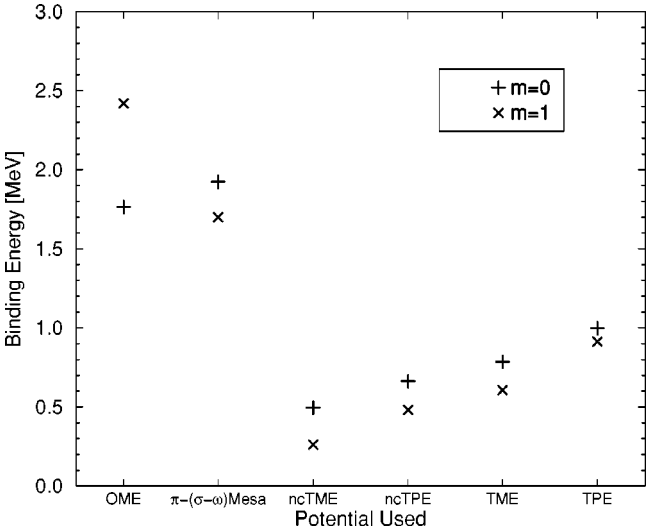

FIG. 8. The values of the binding energy for the $m=0$ and $m=1$ states for different nucleon-nucleon light-front potentials. The σ coupling constant factor is $f_\sigma=1.22$.

In particular, they have used manifestly covariant light-front dynamics to analyze the deuteron. They start with a deuteron wave function calculated in equal-time dynamics, then use a light-front one-pion-exchange potential (expanded to lowest order in powers of $1/M$) to calculate the perturbative corrections to the wave function. They find that the resulting wave function has an unphysical dependence on the orientation of the light-front plane, which would manifest itself as a breaking of rotational invariance in our formalism. They also use the π-σ and π-ω mesa potentials (expanded to lowest order in powers of $1/M$) to calculate the correction to the wave function. When the wave function corrections are combined, they find that the directional dependence of the longest range part of the deuteron wave function cancels exactly.

TABLE II. The values of the binding energy, percentage of the wave function in the D state, and the percentage of the wave function in the $J=1$ state for the $m=0$ and $m=1$ states for different potentials. The σ coupling constant factor is $f_\sigma=1.22$.

Potential	Binding Energy (MeV)			D state (%)		$J=1$ (%)	
	$m=0$	$m=1$	Diff	$m=0$	$m=1$	$m=0$	$m=1$
OME only	−1.7653	−2.4200	0.6547	2.73	3.61	99.99	99.96
OME +π-(σ-ω) mesa	−1.9236	−1.7021	−0.2215	2.80	3.38	99.99	99.96
OME +ncTME	−0.4948	−0.2646	−0.2302	1.97	1.76	99.99	99.98
OME +ncTPE	−0.6620	−0.4825	−0.1795	2.16	2.09	99.99	99.98
OME +TME	−0.7861	−0.6060	−0.1801	2.25	2.31	99.99	99.97
OME +TPE	−0.9981	−0.9155	−0.0826	2.42	2.57	99.99	99.98

TABLE III. The values of the binding energy, percentage of the wave function in the D state, and the percentage of the wave function in the $J=1$ state for the $m=0$ and $m=1$ states for different potentials. The σ coupling constant factor is $f_\sigma=1.2815$, distinguishes this table from Table II.

Potential	Binding Energy (MeV)			D state (%)		$J=1$ (%)	
	$m=0$	$m=1$	Diff	$m=0$	$m=1$	$m=0$	$m=1$
OME only	−3.3500	−4.4546	1.1046	3.09	3.97	99.99	99.96
OME $+\pi$-(σ-ω) Mesa	−3.6331	−3.2408	−0.3923	3.10	3.85	99.99	99.95
OME + ncTME	−1.3766	−0.9901	−0.3865	2.67	2.64	99.99	99.97
OME + ncTPE	−1.6532	−1.4693	−0.1839	2.81	2.88	99.99	99.97
OME + TME	−1.8617	−1.6032	−0.2585	2.85	3.05	99.99	99.96
OME + TPE	−2.1915	−2.2137	0.0222	2.95	3.23	99.99	99.97

This implies that for our model, using the π-σ plus π-ω mesa potential [which we denote by π-(σ-ω)] should partially restore the rotational invariance of the deuteron, assuming that the breaking of rotational invariance is due primarily to the one-pion-exchange potential. Note that since we solve for the deuteron wave function self-consistently and to all orders for our potentials, we do not expect to find exactly the same result as Ref. [69].

The first thing to notice about the data in Table II is that the results are essentially the same regardless of if arbitrary angular momentum is used or if the potential is restricted to the $J=1$ sector. The same result is also seen in the pion-only model [46]. It means that the wave functions are numerically approximate to angular momentum eigenstates.

Next we notice the splittings between masses and D-state percentages for the $m=0$ and $m=1$ states. This implies that the states do not transform correctly under rotations. All of the two-meson-exchange potentials used reduce the splittings by similar amounts, by about 60% for the binding energy and by about 70% for the percent D state. Note also that the mass splittings for the pion-only model were much larger [46].

Examining the effects of the individual two-meson-exchange potentials, we see that π-(σ-ω) potential does reduce the mass splitting, but it does not fully remove it. This is expected since the OME potential includes more than just the pion potential, and the potential is relativistic.

Next, we compare the ncTME and ncTPE potentials to the TME and TPE potentials. The nonchiral potentials reduce the binding energy more than the chiral potentials, as we expected from our experience from the pion-only model. However, unlike for the pion-only model, we find that the chiral and nonchiral potential have fairly similar effects [46].

Finally, notice that the mass splitting for the TPE potential is much smaller than for the other two-meson-exchange potentials. By itself, this does not imply that the rotational properties of the deuteron calculated with that potential are significantly better than those from other two-meson-exchange potentials. The individual potentials that make up the TME potential are fairly large in magnitude, but vary in sign. This means that using any subset of those potentials may result in either a larger or smaller mass splitting. In this case, it is smaller. To investigate this further, we examine the currents for the TME and TPE deuteron wave function in Sec. III.

To verify that our results are independent of the value of f_σ, we recalculate the deuteron properties for each of the potentials with $f_\sigma=1.2815$. The results are summarized in Table III, and the binding energies are shown in Fig. 9. The change in f_σ increases the binding of the states, but the rest of the results are qualitatively the same.

We note that we have not analyzed what effect varying the σ-nucleon coupling constants has on computing the scattering $T=0$ scattering phase shifts. A poor representation of the data could cause our computed deuteron form factors to disagree with observations [70].

B. Deuteron form factors

We use the deuteron wave functions obtained for the light-front nucleon-nucleon potential in Sec. II to calculate

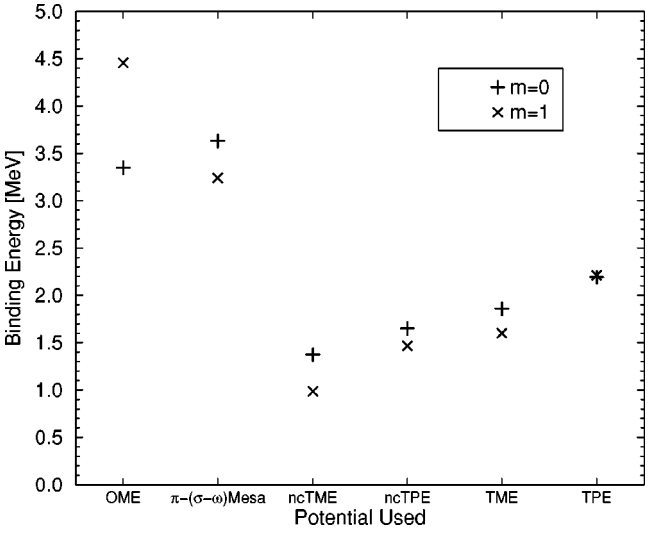

FIG. 9. The values of the binding energy for the $m=0$ and $m=1$ states for different nucleon-nucleon light-front potentials. The σ coupling constant factor is $f_\sigma=1.2815$.

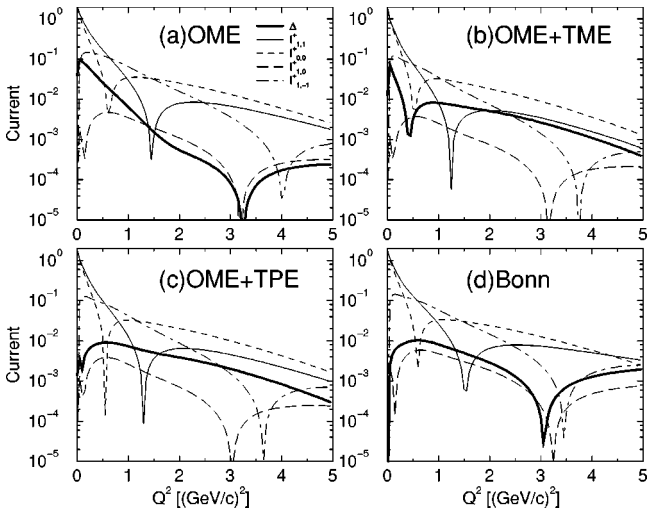

FIG. 10. The matrix elements of $I^+_{(1)m'm}$, the component of the electromagnetic current which multiplies the nucleon F_1 form factor, calculated with the wave function from the (a) OME, (b) OME+TME, (c) OME+TPE, and (d) Bonn potentials.

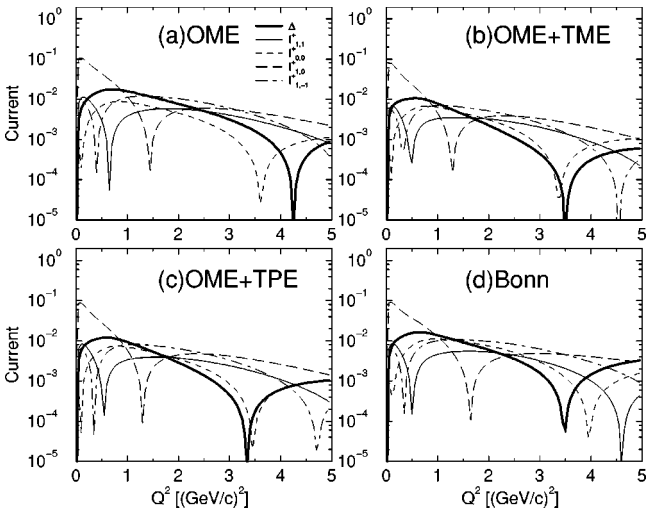

FIG. 11. The matrix elements of $I^+_{(2)m'm}$, the component of the electromagnetic current which multiplies the nucleon F_2 form factor, calculated with the wave function from the (a) OME, (b) OME+TME, (c) OME+TPE, and (d) Bonn potentials.

the deuteron currents and form factors. This gives a solution where light-front dynamics is used consistently throughout. For the potential, we choose the light-front nucleon-nucleon potential with $f_\sigma = 1.2815$. We have verified that the results do not change significantly when $f_\sigma = 1.22$ is used.

Figure 10 shows the currents and the associated angular condition for $I^+_{(1)}$, given by Eq. (54), for several different deuteron wave functions. Results are shown for the wave function from the OME, OME+TME, and OME+TPE potentials (calculated in Sec. II), and the parametrization of the deuteron wave function for the energy independent Bonn potential [23]. The currents matrix elements (but not Δ) are approximately the same regardless of which wave function is used. This consistency is important, since it verifies that the gross features of all the models are the same.

We find that Δ for $I^+_{(1)}$ is much smaller than the largest matrix elements when using the OME wave function. This means that the $I^+_{(1)}$ current transforms very well under rotations. This is somewhat surprising, since we found earlier that the binding energies for the OME wave functions have a large splitting, indicating that OME wave functions transforms poorly under rotations.

Comparing the current calculated with the OME wave function to those calculated with other potentials, we find that for momentum transfers of more than 1 GeV^2 the OME $I^+_{(1)}$ current has the best transformation properties under rotation of all the $I^+_{(1)}$ currents shown.

For smaller momentum transfers, the transformation properties of the Bonn and OME+TME wave functions are the best. This is expected, since in the limit of no momentum transfer, the current $I^+_{(1)m'm}$ is simply the overlap of deuteron wave functions, $\langle m'|m\rangle$. If the initial and final states have the same mass, the matrix element is simply $\delta_{m'm}$, which satisfies the angular condition. However, if the states do not have the same mass (which implies that $m' \neq m$), there will be a nonzero overlap between the two states, which violates the angular condition. Since the masses of the deuteron states are exactly the same for the Bonn wave function, and approximately the same for the OME+TPE wave function, they have a small Δ at low momentum transfer. However, the OME wave functions, having the largest mass splitting, have the largest Δ at low momentum transfers.

Figures 11 and 12 show the current matrix elements and the angular condition for $I^+_{(2)}$ and $I^+_{(5)}$, respectively. The general features of these figures are the same as in Fig. 10, with one important exception. In both figures, the Δ for the OME wave function has about the same magnitude as the Δ's for the other wave functions. This means that the rotational properties of $I^+_{(2)}$ and $I^+_{(5)}$ currents are approximately the same regardless of which wave function is used. This result confirms that the rotational properties of the current matrix elements depend as much on how the current is constructed as they do on which wave function is used.

In Fig. 11, we find that the magnitude of Δ is almost the same as the magnitude of the largest matrix element of $I^+_{(1)}$. This means there is a large deviation from the angular condition, and that form factors calculated with this current may depend strongly on which matrix element is chosen as bad. We show below that this is not the case for the electromagnetic form factors.

We find that Δ is much smaller than the largest matrix element of the axial currents shown in Fig. 12 for most values of momentum transfer. This means that the deuteron axial form factor will be essentially independent of which matrix element is chosen as bad, except for within the range of 1.5 to 2 GeV^2.

Now we combine the two parts of the electromagnetic current, $I^+_{(1)}$ and $I^+_{(2)}$, with the nucleon form factors F_1 and F_2 to get the total current. Figure 13 shows the currents for $F_1 I^+_{(1)}$ and $F_2 I^+_{(2)}$, as well as the sum, I^+. The Gari:1985 nucleon form factors are used [61]. We find that $F_1 I^+_{(1)}$ gives the largest contribution to the total current, and because Δ is

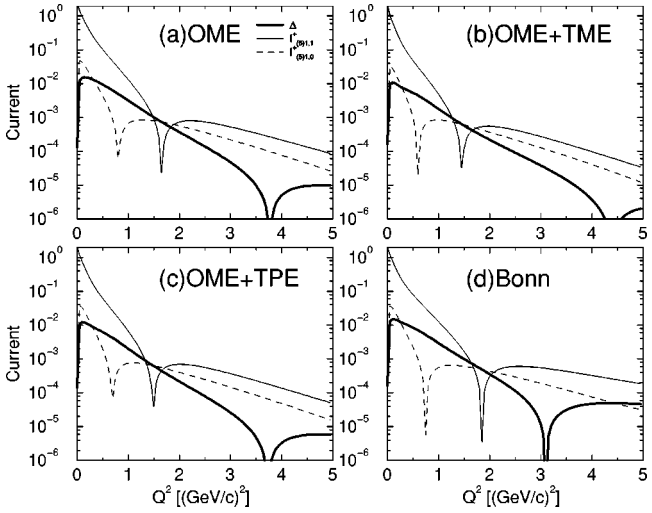

FIG. 12. The matrix elements of $I^{+}_{(5)m'm}$, the deuteron axial current including the nucleon axial form factor, calculated with the wave function from the (a) OME, (b) OME+TME, (c) OME +TPE, and (d) Bonn potentials.

small for $I^{+}_{(1)}$, Δ is also small for the total current, meaning that the total current transforms well under rotations. Thus, in spite of the fact that Δ is approximately the same size as the current matrix elements for $I^{+}_{(2)}$, the deuteron electromagnetic form factors should not depend too strongly on the choice of the bad matrix element. This is especially true for the form factors calculated with the OME wave function.

We calculate the form factors A, B, T_{20}, and F_A using the OME wave function, and show the results in Fig. 14. The definitions of the bad matrix elements are given in Secs. III A 4 and III B. In general, the form factors do not depend strongly on which matrix element is chosen as bad, in agreement what what we predicted in the previous paragraph. The only exception is for the B form factor, and to a lesser extent the F_A form factor, near where they cross zero. This is not

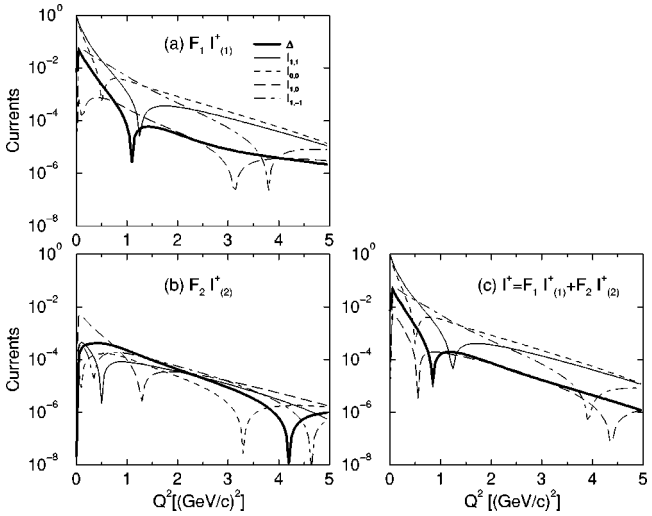

FIG. 13. The matrix elements for $F_1 I^{+}_{(1)m'm}$, $F_2 I^{+}_{(2)m'm}$, and $I^{+}_{m'm}$ calculated with the OME wave functions. The Gari:1985 nucleon isoscalar form factors are used for F_1 and F_2.

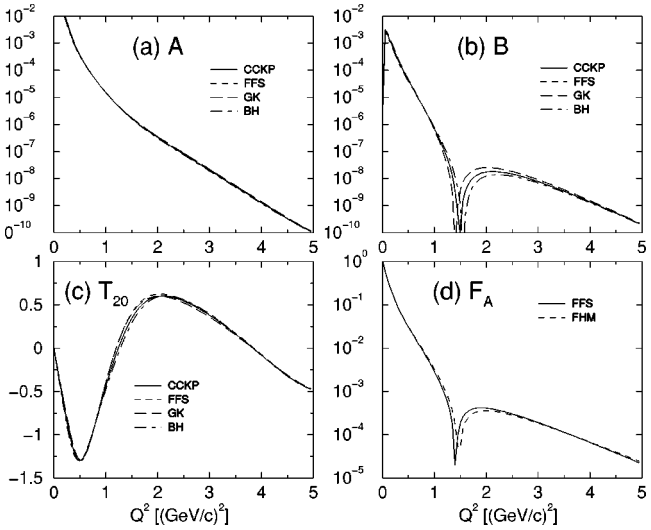

FIG. 14. The form factors A, B, T_{20}, and F_A calculated using the various choices of the bad matrix element. The OME wave function is used, along with the Lomon nucleon form factors for the electromagnetic form factors, and the Liesenfeld nucleon form factor for the axial form factor.

too surprising, since a small constant shift in any function near a zero crossing has a large effect in a logarithmic plot. Also, we note that the FFS and CCKP choices of the bad matrix element give the same value for B.

We also use the OME+TME wave function to calculate the form factors A, B, T_{20}, and F_A, which we show in Fig. 15. We argued earlier that these electromagnetic form factors depend more strongly on which matrix element is chosen as bad as those calculated with the OME wave function, and that dependence is clear in this figure. At low momentum transfers, the dependence on the change is fairly small, but as

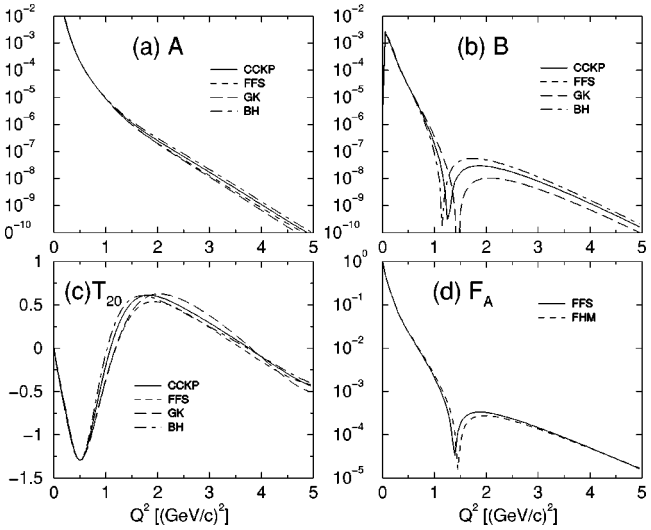

FIG. 15. The form factors A, B, T_{20}, and F_A calculated using the various choices of the bad matrix element. The definitions of the bad matrix elements are given in Secs. III A 4 and III B. The OME+TME wave function is used, along with the Lomon nucleon form factors for the electromagnetic form factors, and the Liesenfeld nucleon form factor for the axial form factor.

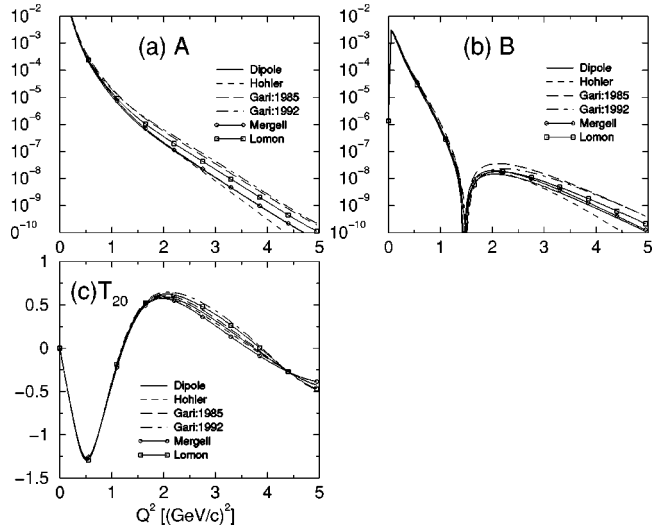

FIG. 16. The electromagnetic form factors *A*, *B*, and T_{20} calculated using the various choices of the nucleon isoscalar form factors. The OME wave function is used, along with the FFS choice of the bad deuteron current matrix. The axial form factor is not shown since its dependence on different form factors is trivial.

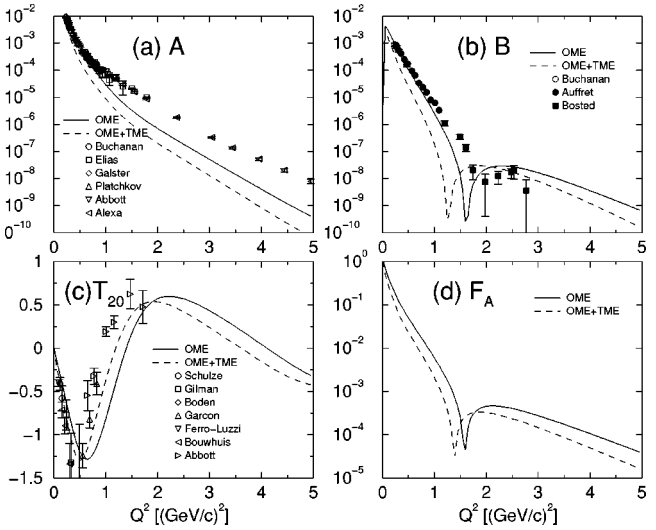

FIG. 17. The *A*, *B*, T_{20}, and F_A form factors for the OME and OME+TME potentials, along with data. See the accompanying text for an explanation of the data.

the momentum transfer increases, so does the dependence. The axial form factor is not affected as strongly, primarily because each wave function generates an axial current which violates the angular condition by approximately the same amount.

Since there are many different models of the nucleon electromagnetic form factors, we calculate the deuteron electromagnetic form factors using each of them to see what effect the differences have. The results are shown in Fig. 16. At low momentum transfers, all the nucleon form factors give close to the same results. However, when the momentum transfers is large, we find a large spread in the values due to nucleon form factors. In fact, this spread is larger than the spread of values obtained from using different bad matrix elements with the OME+TME wave functions. In other words, in order to obtain accurate results for momentum transfers over 2 GeV^2, it is more important to determine which nucleon form factor to use than when bad matrix to use.

Finally, in Fig. 17, we compare the *A*, *B*, T_{20}, and F_A form factors for the OME and OME+TME wave functions to experimental data. The bad component was chosen according to FFS, and the nucleon form factors of Lomon were used for *A*, *B*, and T_{20}, while the Liesenfeld axial nucleon form factor was used for F_A. The data for *A* is from: Buchanan *et al.* [71], Elias *et al.* [72], Galster *et al.* [73], Platchkov *et al.* [74], Abbott *et al.* [75], and Alexa *et al.* [1]; the data for *B* is from: Buchanan *et al.* [71], Auffret *et al.* [76], and Bosted *et al.* [77]; and the data for T_{20} is from: Schulze *et al.* [78], Gilman *et al.* [79], Boden *et al.* [80], Garcon *et al.* [81], Ferro-Luzzi *et al.* [82], Bouwhuis *et al.* [83], and Abbott *et al.* [84].

There is a rather large difference between the form factors calculated with the OME and OME+TME wave functions. This difference is due primarily to the fact that the OME wave functions are more deeply bound than the OME+TME wave functions, and it can be reduced by choosing a different sigma coupling constant f_σ for the OME and OME+TME potentials. However, for our analysis of rotational invariance, it is important to keep f_σ fixed.

The difference between the calculated form factors and the data is also quite large. This is not unexpected, since in our model of the current, meson exchange currents are not included. It is known that these can have a large effect on the form factors at large momentum transfers [55,85,86]. Including these effects could bring the form factors into better agreement with the data. However, we emphasize again that agreement with the data is not a priority of this work. Our goal is to gain a better understanding of the breaking of rotational invariance by the light front, and how to restore that invariance. Only after we have that understanding can we pursue accurate calculation of the form factors with light-front dynamics.

V. CONCLUSIONS

The issue of rotational invariance in light-front dynamics with a fixed-front orientation must be addressed before one attempts to use light-front dynamics for high-precision calculations. In this paper, we find ways to quantify the level to which rotational invariance is broken. We used light-front dynamics to obtain new light-front nucleon-nucleon one-meson-exchange (OME) and two-meson-exchange (TME) potentials. In addition, we examined the rotational properties of wave functions for potentials truncated to different orders.

In Sec. II, we derive OME and TME potentials for a model Lagrangian for nuclear physics which includes chiral symmetry. The deuteron form factors are derived for the wave functions associated with the potentials in Sec. III. Section IV describes our results, starting with the calculation of the binding energies and wave functions for the $m=0$ and $m=1$ states of the deuteron. We find that the splitting between the $m=0$ and $m=1$ states was smaller for the OME

+TME potential as compared to the OME potential.

The wave functions are used to calculate the form factors of the deuteron using only light-front dynamics throughout. In light-front dynamics, there are four independent components of the deuteron current. However, the requirement of rotational invariance introduces an angular condition that the four components must satisfy, reducing the number of physically independent components to three. The deviation of the calculated current components from the angular condition is denoted by Δ. We find that Δ is very small for the deuteron wave functions calculated with the OME potential. This is an important result, since it means that although *in principle* the light-front calculation of the deuteron current calculated with a truncated Hamiltonian and a truncated current operator does not transform correctly under rotations, *in practice* it does quite well. The smallness of Δ means that any reasonable prescription for eliminating the dependent component of the current gives essentially the same results; the uncertainty introduced by the various nucleon form factors is much greater.

We also found that Δ is significantly larger when the TME potentials are used. Since the results in Refs. [19,20,46] indicate that the rotational properties of the TME wave function are better than those for the OME wave function, we interpret the increase in Δ as an indication that extra diagrams need to be included in the current calculation to restore rotational invariance. For example, the component of the current arising from the photon coupling to an intermediate two-meson-exchange type of diagram should, in principle, be included. The inclusion of higher-order terms in the current can be expected to reduce the breaking of rotational invariance of the deuteron form factor.

ACKNOWLEDGMENTS

This work was supported in part by the U.S. Department of Energy under Grant No. DE-FG03-97ER4014. We are grateful to Daniel Phillips for many useful discussions about this work.

APPENDIX: NOTATION, CONVENTIONS, AND USEFUL RELATIONS

For a general four-vector a with components (a^0,a^1,a^2,a^3) in the equal-time basis, we define the light-front variables

$$a^{\pm}=a^0\pm a^3, \tag{A1}$$

$$\boldsymbol{a}_{\perp}=(a^1,a^2), \tag{A2}$$

so the four-vector a^{μ} can be denoted in the light-front basis as

$$a=(a^+,a^-,\boldsymbol{a}_{\perp}). \tag{A3}$$

Using this, we find that the scalar product is

$$a\cdot b=a^{\mu}b_{\mu}=\tfrac{1}{2}(a^+b^-+a^-b^+)-\boldsymbol{a}_{\perp}\cdot\boldsymbol{b}_{\perp}. \tag{A4}$$

This defines $g_{\mu\nu}$, with $g_{+-}=g_{-+}=1/2$, $g_{11}=g_{22}=-1$, and all other elements of g vanish. The elements of $g^{\mu\nu}$ are obtained from the condition that $g^{\mu\nu}$ is the inverse of $g_{\mu\nu}$, so $g^{\alpha\beta}g_{\beta\lambda}=\delta^{\alpha}_{\lambda}$. Its elements are the same as those of $g_{\mu\nu}$, except that $g^{-+}=g^{+-}=2$. Thus,

$$a^{\pm}=2a_{\mp}. \tag{A5}$$

and the partial derivatives are similarly given by

$$\partial^{\pm}=2\partial_{\mp}=2\frac{\partial}{\partial x^{\mp}}. \tag{A6}$$

To find the physical consequences of this coordinate system, consider the commutation relations $[p^{\mu},x^{\nu}]=ig^{\mu\nu}$, which yield

$$[p^{\pm},x^{\mp}]=2i, \tag{A7}$$

$$[\boldsymbol{p}^i_{\perp},\boldsymbol{x}^j_{\perp}]=-i\delta_{i,j}, \tag{A8}$$

with the other commutators equal to zero. This means that $\boldsymbol{x}^i_{\perp}$ is canonically conjugate to $\boldsymbol{p}^i_{\perp}$, and $x^{\pm}$ is conjugate to $p^{\mp}$. Since x^+ plays the role of time (the light-front time) in light-front dynamics, and p^- is canonically conjugate to x^+, this means that p^- is the light-front energy and that the light-front Hamiltonian is given by P^-.

In any Hamiltonian theory, particles have an energy defined by the on-shell constraint $k^2=m^2$. This implies that the light-front energy of a particle is

$$k^-=\frac{m^2+\boldsymbol{k}^2_{\perp}}{k^+}. \tag{A9}$$

The independent components of the momentum can be written as a light-front three-vector $\boldsymbol{k}_{\mathrm{LF}}$, denoted by

$$\boldsymbol{k}_{\mathrm{LF}}=(k^+,\boldsymbol{k}_{\perp}). \tag{A10}$$

For dealing with spin, we require the Pauli sigma matrices, which are

$$(\sigma^1,\sigma^2,\sigma^3)=\left(\begin{pmatrix}0&1\\1&0\end{pmatrix},\begin{pmatrix}0&-i\\i&0\end{pmatrix},\begin{pmatrix}1&0\\0&-1\end{pmatrix}\right). \tag{A11}$$

The Bjorken and Drell convention [87] for the gamma matrices is used in this work. They specify that

$$\gamma^0=\beta=\begin{pmatrix}1&0\\0&-1\end{pmatrix}, \tag{A12}$$

$$\boldsymbol{\gamma}=\beta\boldsymbol{\alpha}=\begin{pmatrix}0&\sigma\\-\sigma&0\end{pmatrix}, \tag{A13}$$

$$\gamma^5=i\gamma^0\gamma^1\gamma^2\gamma^3=\begin{pmatrix}0&1\\1&0\end{pmatrix}. \tag{A14}$$

The spin matrices S^i then are

$$S^i=\frac{1}{2}\Sigma^i=-\frac{1}{2}\gamma^5\gamma^i, \tag{A15}$$

$$\Sigma^i=\begin{pmatrix}\sigma^i & 0\\ 0 & -\sigma^i\end{pmatrix}. \tag{A16}$$

Using $\mathbf{\Sigma}$, we can express the helicity operator as $H=\hat{p}\cdot\mathbf{\Sigma}$, which has eigenvalues ± 1. This is useful since the helicity is invariant under rotations.

It is useful to define the spinor projection operators $\Lambda_\pm$ by

$$\Lambda_\pm=\frac{1}{4}\gamma^\mp\gamma^\pm=\frac{1}{2}\gamma^0\gamma^\pm=\frac{1}{2}(I\pm\alpha^3). \tag{A17}$$

These satisfy the requirements for projection operators,

$$\Lambda_+ +\Lambda_- =1, \tag{A18}$$

$$(\Lambda_\pm)^2=\Lambda_\pm, \tag{A19}$$

$$\Lambda_\pm\Lambda_\mp=0. \tag{A20}$$

We summarize the effect these projection operators have on the gamma matrices:

$$\Lambda_\pm\gamma^0=\gamma^0\Lambda_\mp, \tag{A21}$$

$$\Lambda_\pm\gamma^\pm=0=\gamma^\pm\Lambda_\mp, \tag{A22}$$

$$\Lambda_\pm\gamma^\mp=\gamma^\mp=\gamma^\mp\Lambda_\mp, \tag{A23}$$

$$\Lambda_\pm\gamma^\perp=\gamma^\perp\Lambda_\pm, \tag{A24}$$

and under conjugation,

$$\gamma^0\Lambda_\pm^\dagger\gamma^0=\Lambda_\mp. \tag{A25}$$

The light-front spinors are defined to be [6]

$$u_{\rm LF}(k,m)\equiv\frac{1}{\sqrt{Mk^+}}[M\Lambda_-+(k^+ +\boldsymbol{\alpha}^\perp\cdot\mathbf{k}^\perp)\Lambda_+]\chi_{{\rm LF},m} \tag{A26}$$

$$=\frac{1}{\sqrt{Mk^+}}[\Lambda_-(M+\boldsymbol{\alpha}^\perp\cdot\mathbf{k}^\perp)+\Lambda_+k^+]\chi_{{\rm LF},m}, \tag{A27}$$

$$\chi_{{\rm LF},m}\equiv\begin{pmatrix}\chi_m\\ 0\end{pmatrix}, \tag{A28}$$

where χ_m is the usual Pauli spinor, and the $\Lambda_\pm$ are the spinor projection operators defined in Eq. (A17). We find that

$$\overline{u}_{\rm LF}(k,m)=\frac{1}{\sqrt{Mk^+}}\chi^\dagger_{{\rm LF},m}[\Lambda_+M+\Lambda_-(k^+ +\boldsymbol{\alpha}^\perp\cdot\mathbf{k}^\perp)] \tag{A29}$$

$$=\frac{1}{\sqrt{Mk^+}}\chi^\dagger_{{\rm LF},m}[(M-\boldsymbol{\alpha}^\perp\cdot\mathbf{k}^\perp)\Lambda_+ +k^+\Lambda_-]. \tag{A30}$$

Note that these spinors are normalized to satisfy $\overline{u}_{\rm LF}(k,m')u_{\rm LF}(k,m)=\delta_{m'm}$.

For helicity spinors, we choose the eigenvectors of the helicity operator $(\boldsymbol{\sigma}\cdot\hat{\boldsymbol{p}})$ as the χ's. In particular, $(\hat{\boldsymbol{p}}\cdot\mathbf{\Sigma})u(\boldsymbol{p},\lambda)=hu(\boldsymbol{p},\lambda)$, where $h=2\lambda$. This choice allows us to write

$$u(\boldsymbol{p},\lambda)=\sqrt{\frac{W}{2M}}\begin{pmatrix}1\\ f\end{pmatrix}\chi_\lambda(\hat{\boldsymbol{p}}), \tag{A31}$$

and

$$\chi_\lambda(\hat{\boldsymbol{p}})=\begin{cases}\begin{pmatrix}c_2e^{-i\phi/2}\\ s_2e^{+i\phi/2}\end{pmatrix} & \text{if } h=+1\\ \begin{pmatrix}-s_2e^{-i\phi/2}\\ c_2e^{+i\phi/2}\end{pmatrix} & \text{if } h=-1\end{cases}, \tag{A32}$$

where $c_2=\cos(\theta/2)$, $s_2=\sin(\theta/2)$, $f=hp/W$, and $h=2\lambda$.

When there are two fermions in the center-of-momentum frame, we can define $\phi\equiv\phi_1$ and $\theta\equiv\theta_1$ and for particle two $\phi_2=\pi+\phi$ and $\theta_2=\pi-\theta$. This means that

$$u(\boldsymbol{p}_i,\lambda_i)=\sqrt{\frac{W}{2M}}\begin{pmatrix}1\\ f_i\end{pmatrix}\chi_{i,\lambda_i}(\hat{\boldsymbol{p}}), \tag{A33}$$

where $i=1,2$ and

$$\chi_{1,\lambda_1}(\hat{\boldsymbol{p}})=\chi_{\lambda_1}(\hat{\boldsymbol{p}}), \tag{A34}$$

$$\chi_{2,\lambda_2}(\hat{\boldsymbol{p}})=i\chi_{-\lambda_2}(\hat{\boldsymbol{p}}). \tag{A35}$$

[1] L.C. Alexa *et al.*, Phys. Rev. Lett. **82**, 1374 (1999).
[2] P.A.M. Dirac, Rev. Mod. Phys. **21**, 392 (1949).
[3] S.J. Brodsky, H.-C. Pauli, and S.S. Pinsky, Phys. Rep. **301**, 299 (1998).
[4] A. Harindranath, hep-ph/9612244.
[5] T. Heinzl, hep-th/9812190.
[6] G.A. Miller, Phys. Rev. C **56**, 2789 (1997).
[7] G.A. Miller, Prog. Part. Nucl. Phys. **45**, 83 (2000).
[8] This problem is not unique to light-front dynamics. In the canonical form of Hamiltonian dynamics (equal-time dynamics), four of the Poincaré group generators are dynamic, and thus complicated.
[9] F. Coester, Prog. Part. Nucl. Phys. **29**, 1 (1992).
[10] U. Trittmann and H.-C. Pauli, hep-th/9705021.
[11] L.L. Frankfurt, T. Frederico, and M. Strikman, Phys. Rev. C **48**, 2182 (1993).
[12] T. Frederico, E.M. Henley, and G.A. Miller, Nucl. Phys. **A533**, 617 (1991).
[13] L.A. Kondratyuk and M.I. Strikman, Nucl. Phys. **A426**, 575 (1984).

[14] F. Cardarelli, I.L. Grach, I.M. Narodetsky, G. Salme, and S. Simula, Phys. Lett. B **349**, 393 (1995).
[15] D. Arndt and C.-R. Ji, Phys. Rev. D **60**, 094020 (1999).
[16] J. Carbonell and V.A. Karmanov, in *Williamsburg 1994, Few-Body Problems in Physics*, edited by F. Gross (American Institute of Physics, New York, 1995) pp. 891–894.
[17] J. Carbonell and V.A. Karmanov, Nucl. Phys. **A581**, 625 (1995).
[18] P.L. Chung, W.N. Polyzou, F. Coester, and B.D. Keister, Phys. Rev. C **37**, 2000 (1988).
[19] J.R. Cooke, G.A. Miller, and D.R. Phillips, Phys. Rev. C **61**, 064005 (2000).
[20] J.R. Cooke and G.A. Miller, Phys. Rev. C **62**, 054008 (2000).
[21] G.A. Miller and R. Machleidt, Phys. Rev. C **60**, 035202 (1999).
[22] F. Gursey, Nuovo Cimento **16**, 230 (1960).
[23] R. Machleidt, K. Holinde, and C. Elster, Phys. Rep. **149**, 1 (1987).
[24] R. Machleidt, in *Computational Nuclear Physics 2—Nuclear Reactions*, edited by K. Langanke, J. A. Maruhn, and S. E. Koonin (Springer, New York, 1993), Chap. 1, p. 1.
[25] D. Black, A.H. Fariborz, F. Sannino, and J. Schechter, Phys. Rev. D **59**, 074026 (1999).
[26] D. Black, A.H. Fariborz, and J. Schechter, Phys. Rev. D **61**, 074030 (2000).
[27] D. Black, A.H. Fariborz, S. Moussa, S. Nasri, and J. Schechter, Phys. Rev. D **64**, 014031 (2001).
[28] G.A. Miller, Phys. Rev. C **56**, 8 (1997).
[29] S.-J. Chang, R.G. Root, and T.-M. Yan, Phys. Rev. D **7**, 1133 (1973).
[30] S.-J. Chang and T.-M. Yan, Phys. Rev. D **7**, 1147 (1973).
[31] T.-M. Yan, Phys. Rev. D **7**, 1760 (1973).
[32] T.-M. Yan, Phys. Rev. D **7**, 1780 (1973).
[33] J.R. Cooke, Ph.D. thesis, University of Washington, 2001.
[34] D.E. Soper, SLAC-R-0137.
[35] J.B. Kogut and D.E. Soper, Phys. Rev. D **1**, 2901 (1970).
[36] J.D. Bjorken, J.B. Kogut, and D.E. Soper, Phys. Rev. D **3**, 1382 (1971).
[37] D.E. Soper, Phys. Rev. D **4**, 1620 (1971).
[38] Y. Nambu, Prog. Theor. Phys. **5**, 614 (1950).
[39] J. Schwinger, Proc. Natl. Acad. Sci. U.S.A. **37**, 452 (1951).
[40] J. Schwinger, Proc. Natl. Acad. Sci. U.S.A. **37**, 455 (1951).
[41] M. Gell-Mann and F. Low, Phys. Rev. **84**, 350 (1951).
[42] E.E. Salpeter and H.A. Bethe, Phys. Rev. **84**, 1232 (1951).
[43] N.C.J. Schoonderwoerd and B.L.G. Bakker, Phys. Rev. D **57**, 4965 (1998).
[44] N.C.J. Schoonderwoerd and B.L.G. Bakker, Phys. Rev. D **58**, 025013 (1998).
[45] N. Schoonderwoerd, Ph.D. thesis, Vrije University, 1998.
[46] J.R. Cooke and G.A. Miller, Phys. Rev. C **65**, 067001 (2002).
[47] E. Hummel and J.A. Tjon, Phys. Rev. C **42**, 423 (1990).
[48] M.J. Zuilhof and J.A. Tjon, Phys. Rev. C **22**, 2369 (1980).
[49] G. Rupp and J.A. Tjon, Phys. Rev. C **41**, 472 (1990).
[50] M. Garcon and J.W. Van Orden, nucl-th/0102049.
[51] R.G. Arnold, C.E. Carlson, and F. Gross, Phys. Rev. C **23**, 363 (1981).
[52] F. Coester and A. Ostebee, Phys. Rev. C **11**, 1836 (1975).
[53] T.E.O. Ericson and M. Rosa-Clot, Nucl. Phys. **A405**, 497 (1983).
[54] P.J. Mohr and B.N. Taylor, Rev. Mod. Phys. **72**, 351 (2000).
[55] D.R. Phillips, S.J. Wallace, and N.K. Devine, Phys. Rev. C **58**, 2261 (1998).
[56] R. Dashen and M. Gell-Mann, Phys. Rev. Lett. **17**, 340 (1966).
[57] H.J. Melosh, Phys. Rev. D **9**, 1095 (1974).
[58] I.L. Grach and L.A. Kondratyuk, Yad. Fiz. **39**, 316 (1984) [Sov. J. Nucl. Phys. **39**, 198 (1984)].
[59] S.J. Brodsky and J.R. Hiller, Phys. Rev. D **46**, 2141 (1992).
[60] G. Hohler *et al.*, Nucl. Phys. **B114**, 505 (1976).
[61] M.F. Gari and W. Krümpelmann, Z. Phys. A **322**, 689 (1985).
[62] M.F. Gari and W. Krümpelmann, Phys. Lett. B **274**, 159 (1992).
[63] M.F. Gari and W. Krümpelmann, Phys. Lett. B **282**, 483 (1992).
[64] P. Mergell, U.G. Meissner, and D. Drechsel, Nucl. Phys. **A596**, 367 (1996).
[65] E.L. Lomon, Phys. Rev. C **64**, 035204 (2001).
[66] K. de Jager, hep-ex/0003034.
[67] M. Burkardt, Phys. Rev. D **54**, 2913 (1996).
[68] A. Liesenfeld *et al.*, Phys. Lett. B **468**, 20 (1999).
[69] J. Carbonell, B. Desplanques, V.A. Karmanov, and J.F. Mathiot, Phys. Rep. **300**, 215 (1998).
[70] G.A. Miller and M. Strikman, nucl-th/0105015.
[71] C.D. Buchanan *et al.*, Phys. Rev. Lett. **15**, 303 (1965).
[72] J.E. Elias *et al.*, Phys. Rev. **177**, 2075 (1969).
[73] S. Galster *et al.*, Nucl. Phys. **B32**, 221 (1971).
[74] S. Platchkov *et al.*, Nucl. Phys. **A510**, 740 (1990).
[75] D. Abbott *et al.*, Phys. Rev. Lett. **82**, 1379 (1999).
[76] S. Auffret *et al.*, Phys. Rev. Lett. **54**, 649 (1985).
[77] P. Bosted *et al.*, Phys. Rev. C **42**, 38 (1990).
[78] M.E. Schulze *et al.*, Phys. Rev. Lett. **52**, 597 (1984).
[79] R. Gilman *et al.*, Phys. Rev. Lett. **65**, 1733 (1990).
[80] B. Boden *et al.*, Z. Phys. C **49**, 175 (1991).
[81] M. Garcon *et al.*, Phys. Rev. C **49**, 2516 (1994).
[82] M. Ferro-Luzzi *et al.*, Phys. Rev. Lett. **77**, 2630 (1996).
[83] M. Bouwhuis *et al.*, Phys. Rev. Lett. **82**, 3755 (1999).
[84] D. Abbott *et al.*, Phys. Rev. Lett. **84**, 5053 (2000).
[85] R.B. Wiringa, V.G.J. Stoks, and R. Schiavilla, Phys. Rev. C **51**, 38 (1995).
[86] R. Schiavilla and D.O. Riska, Phys. Rev. C **43**, 437 (1991).
[87] J.D. Bjorken and S.D. Drell, *Relativistic Quantum Mechanics* (McGraw-Hill, New York, 1964), Chap. 3.